



National Library  
of Canada

Bibliothèque nationale  
du Canada

Canadian Theses Service

Services des thèses canadiennes

Ottawa, Canada  
K1A 0N4

## CANADIAN THESES

### NOTICE

The quality of this microfiche is heavily dependent upon the quality of the original thesis submitted for microfilming. Every effort has been made to ensure the highest quality of reproduction possible.

If pages are missing, contact the university which granted the degree.

Some pages may have indistinct print especially if the original pages were typed with a poor typewriter ribbon or if the university sent us an inferior photocopy.

Previously copyrighted materials (journal articles, published tests, etc.) are not filmed.

Reproduction in full or in part of this film is governed by the Canadian Copyright Act, R.S.C. 1970, c. C-30. Please read the authorization forms which accompany this thesis.

**THIS DISSERTATION  
HAS BEEN MICROFILMED  
EXACTLY AS RECEIVED**

## THÈSES CANADIENNES

### AVIS

La qualité de cette microfiche dépend grandement de la qualité de la thèse soumise au microfilmage. Nous avons tout fait pour assurer une qualité supérieure de reproduction.

S'il manque des pages, veuillez communiquer avec l'université qui a conféré le grade.

La qualité d'impression de certaines pages peut laisser à désirer, surtout si les pages originales ont été dactylographiées à l'aide d'un ruban usé ou si l'université nous a fait parvenir une photocopie de qualité inférieure.

Les documents qui font déjà l'objet d'un droit d'auteur (articles de revue, examens publiés, etc.) ne sont pas microfilmés.

La reproduction, même partielle, de ce microfilm est soumise à la Loi canadienne sur le droit d'auteur, SRC 1970, c. C-30. Veuillez prendre connaissance des formules d'autorisation qui accompagnent cette thèse.

**LA THÈSE A ÉTÉ  
MICROFILMÉE TELLE QUE  
NOUS L'AVONS REÇUE**

**Canada**



National Library  
of Canada

Bibliothèque nationale  
du Canada

0-315-23253-6

Canadian Theses Division

Division des thèses canadiennes

Ottawa, Canada  
K1A 0N4

### PERMISSION TO MICROFILM — AUTORISATION DE MICROFILMER

• Please print or type — Écrire en lettres moulées ou dactylographier

Full Name of Author — Nom complet de l'auteur

SATHYA MANGALAM RAMASWAMY VENKATRAMANAN

Date of Birth — Date de naissance

APRIL 12, 1952

Country of Birth — Lieu de naissance

INDIA

Permanent Address — Résidence fixe

31 KITTASWAMY STREET  
GOSICHERTICALAYAM  
TAMIL NADU 638452  
INDIA

Title of Thesis — Titre de la thèse

COMPUTER ENHANCEMENT OF  
ECG CARDIOGRAPHIC IMAGES

University — Université

UNIVERSITY OF ALBERTA

Degree for which thesis was presented — Grade pour lequel cette thèse fut présentée

MASTERS OF SCIENCE

Year this degree conferred — Année d'obtention de ce grade

1984

Name of Supervisor — Nom du directeur de thèse

DR. V. A. BAVIS

Permission is hereby granted to the NATIONAL LIBRARY OF CANADA to microfilm this thesis and to lend or sell copies of the film.

The author reserves other publication rights, and neither the thesis nor extensive extracts from it may be printed or otherwise reproduced without the author's written permission.

L'autorisation est, par la présente, accordée à la BIBLIOTHÈQUE NATIONALE DU CANADA de microfilmer cette thèse et de prêter ou de vendre des exemplaires du film.

L'auteur se réserve les autres droits de publication; ni la thèse ni de longs extraits de celle-ci ne doivent être imprimés ou autrement reproduits sans l'autorisation écrite de l'auteur.

Date

SEP 25, 1984

Signature

THE UNIVERSITY OF ALBERTA

Computer Enhancement of Echocardiographic Images

by

S. R. Venkatramanan



A THESIS

SUBMITTED TO THE FACULTY OF GRADUATE STUDIES AND RESEARCH  
IN PARTIAL FULFILMENT OF THE REQUIREMENTS FOR THE DEGREE  
OF Master of Science

Department of Computing Science

EDMONTON, ALBERTA

Fall 1985

THE UNIVERSITY OF ALBERTA

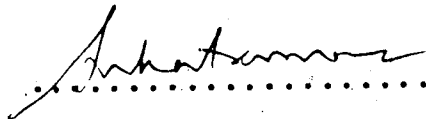
RELEASE FORM

NAME OF AUTHOR            S. R. Venkatramanan  
TITLE OF THESIS            Computer Enhancement of  
                                 Echocardiographic Images  
DEGREE FOR WHICH THESIS WAS PRESENTED    Master of Science  
YEAR THIS DEGREE GRANTED    Fall 1985

Permission is hereby granted to THE UNIVERSITY OF ALBERTA LIBRARY to reproduce single copies of this thesis and to lend or sell such copies for private, scholarly or scientific research purposes only.

The author reserves other publication rights, and neither the thesis nor extensive extracts from it may be printed or otherwise reproduced without the author's written permission.

(SIGNED) .....



PERMANENT ADDRESS:

31 Kittasamy Street  
Gobichettipalayam  
Tamil Nadu, 638 452 INDIA

DATED August 14, ..... 1985

THE UNIVERSITY OF ALBERTA  
FACULTY OF GRADUATE STUDIES AND RESEARCH

The undersigned certify that they have read, and recommend to the Faculty of Graduate Studies and Research, for acceptance, a thesis entitled Computer Enhancement of Echocardiographic Images submitted by S. R. Venkatramanan in partial fulfilment of the requirements for the degree of Master of Science.

Wayne H. Daws  
.....

Supervisor

Masayoshi Aoi  
.....

McAelli  
.....

K. Blument  
.....

W. Armstrong  
.....

Date August 14, 1985  
.....

## ABSTRACT

This thesis attempts to analyze ultrasonic images of human hearts. A multistep procedure is described for enhancing the echocardiograms. The procedure consists of three main steps: smoothing, edge detection and contour tracking. The results are illustrated at each step for two frames chosen at random. Several noise filtering algorithms are presented and their performance compared. Edge operators found in the literature are discussed with respect to their relative merits. Modification to one of them is proposed that gives better results for the images under consideration. A few contour tracking algorithms are studied and an algorithm which combines the best features of two of them is presented. The procedure also consists of steps for: enhancing the image, reducing the processing time, compression of the image, encoding of the data and expanding the processed image to its original size.

## ACKNOWLEDGEMENTS

First, I would like to thank Dr. Wayne Davis for his supervision of this work, continued support and helpful comments at various instants. I would also like to thank Dr. B. I. Jugdutt for providing video tapes of echocardiograms and Mr. Robert Heath for helping in digitizing them. The thesis examining committee consisting of Drs. T. M. Caelli, L. K. Schubert, W. W. Armstrong and M. Aoki is very much appreciated for the critical review of this work. Thanks are also due to the staff of the Department of Computing Science for providing me with much needed technical support during this project. I have to thank the Department of Computing Science for providing me with financial support in the form of Teaching Assistantship and the National Science and Engineering Research Council for supporting this work under the grant NSERC A7634. Lastly, but it is very important, I have to acknowledge the patience and understanding my wife, Usha, has shown to me throughout the period of this research. But for her co-operation this work could never have taken this shape.

## Table of Contents

Chapter	Page
1. INTRODUCTION .....	1
1.1 BACKGROUND .....	2
1.2 SPECIFIC PROBLEMS .....	5
1.3 ORGANIZATION .....	6
2. ULTRASONIC ECHOCARDIOGRAPHY .....	8
2.1 PHYSICS OF ULTRASONIC TRANSDUCERS .....	8
2.2 IMAGING MODES .....	11
2.3 LIMITATIONS OF SINGLE BEAM TRANSDUCERS .....	12
2.4 TWO DIMENSIONAL IMAGING .....	14
3. NOISE FILTERING .....	18
3.1 EXISTING METHODS .....	19
3.2 EXTRACTION OF REGION OF INTEREST .....	21
3.3 MEDIAN FILTER .....	23
3.4 AVERAGING .....	25
3.4.1 Unweighted Averaging .....	27
3.4.2 Weighted Averaging .....	28
3.4.2.1 Spatial Weights .....	28
3.4.2.2 Gray Level Weighting .....	32
3.4.2.3 Double Weighted Smoothing .....	36
3.5 COMPARISON OF RESULTS .....	39
3.6 CONCLUSION .....	40
4. EDGE DETECTION .....	42
4.1 IMAGE COMPRESSION .....	43
4.2 HISTOGRAM STRETCHING .....	44
4.3 SECOND LEVEL SMOOTHING .....	46



4.4	GRADIENT ALGORITHMS .....	46
4.5	THE ROBERTS OPERATOR .....	47
4.6	BEST-FIT EDGE OPERATOR .....	48
4.7	EXTENDED BEST-FIT EDGE OPERATOR .....	49
4.8	WEIGHTED OPERATOR OVER 3 x 3 NEIGHBORHOOD .....	50
4.9	ELECTROSTATIC CHARGE ANALOGY .....	51
4.10	EXTENSION OF THE ABOVE OPERATOR .....	52
4.11	COMPARISON AND CONCLUSION .....	55
5.	CONTOUR TRACING .....	61
5.1	TRACING WITH A-MODE AND M-MODE IMAGES .....	62
5.2	CONTOURS IN THE TRANSFORMED IMAGES .....	65
5.3	CONTOURS WITHOUT IMAGE TRANSFORMS .....	66
5.3.1	Region Boundaries .....	66
5.3.2	Adaptive Threshold Boundary Detection .....	67
5.3.3	Restricted Search with Fixed Threshold .....	69
5.3.4	Restricted Search with Adaptive Threshold .....	71
5.4	CONTOUR EXPANSION .....	73
5.5	CONCLUSION .....	77
6.	CONCLUSION .....	78
6.1	STUDY OF THE CURRENT STATE OF ART .....	78
6.2	CONTRIBUTION OF THIS RESEARCH TO IMAGE PROCESSING .....	80
6.3	CRITICAL REVIEW .....	83
6.4	LIMITATIONS OF THE PROPOSED PROCEDURE .....	85
6.5	DIRECTIONS FOR FURTHER RESEARCH .....	87

REFERENCES .....	90
APPENDIX A .....	95

List of Tables

Table	Page
3.1 Comparison of noise filters .....	40

## List of Figures

Figure	Page
2.1	Block Diagram of basic Phased-Array System .....16
2.2	Phased array radiating a plane wave at an angle $\theta$ with a velocity $V$ .....16
2.3	Phased array radiating a wave focused at a point P .....16
2.4	A Cross section of the heart .....17
3.1	Averaging masks .....34
5.1	Contour tracing with A-mode and M-mode images .....63
5.2	Order of search directions .....70

## List of Plates

Plate	Page
3.1 Original echocardiogram of Frame 1 .....	22
3.2 ROI in echocardiogram - frame 1 .....	24
3.3 ROI in echocardiogram - frame 2 .....	24
3.4 Median filter output for frame 1 .....	26
3.5 Median filter output for frame 2 .....	26
3.6 3 x 3 unweighted averaging output for frame 1 .....	29
3.7 3 x 3 unweighted averaging output for frame 2 .....	29
3.8 Output of 5 x 5 unweighted averaging on frame 1 .....	30
3.9 Output of 5 x 5 unweighted averaging on frame 2 .....	30
3.10 Spatial weighted filter output for frame 1 .....	33
3.11 Spatial weighted filter output for frame 2 .....	33
3.12 Gray level weighted filter output for frame 1 .....	35
3.13 Gray level weighted filter output for frame 2 .....	35
3.14 Output of filter with both weights - frame 1 .....	37
3.15 Output of filter with both weights - frame 2 .....	37
4.1 Frame 1 is (a) Compressed (b) Histogram stretched .....	45
4.2 Output of Sethi's operator for frame 1 .....	53
4.3 Output of Sethi's operator for frame 2 .....	53
4.4 New operator output for frame 1 .....	56
4.5 New operator output for frame 2 .....	56

Plate	Page
5.1	Contour for frame 1 with new algorithm .....74
5.2	Contour for frame 2 with new algorithm .....74
5.3	Contour superimposed on original - Frame 1 .....75
5.4	Contour superimposed on ROI - Frame 2 .....75
5.5	Contour superimposed on ROI - Frame 3 .....76
5.6	Contour superimposed on ROI - Frame 4 .....76

## CHAPTER 1

### INTRODUCTION

This thesis explores a procedure for an automated analysis of heart images that have been obtained by reflection of ultrasonic waves by the heart. Imaging of the heart serves as a valuable tool in the diagnosis of heart abnormalities and in preventive as well as corrective care of the diseases in the cardiovascular system. During treatment, this would allow cardiologists to monitor the progress of the therapy. Imaging of the heart with reflected sound waves at frequencies higher than the audible range is termed echocardiography. Some heart ailments that otherwise would turn out to be fatal can be easily diagnosed and treated early in their developmental phase with the help of echocardiography.

Safety and reliability are of utmost importance in dealing with human life. The significance of echocardiography in clinical science lies in the following facts: While other means of diagnosis are either hazardous or invasive, echocardiography is relatively safe and non-invasive. Diagnosis using high energy radiation such as X-Rays is hazardous to the body tissues, particularly with prolonged use. The use of a catheter for injecting radioactive dyes in nuclear medicine is an invasive procedure. The patient's emotional and physical conditions

change during these procedures since the patient can be put in pain or discomfort. Thus, procedures like these can by themselves influence the disease and hence can result in incorrect diagnosis. X-ray and CT techniques bring out only the anatomy of the organs under study and not any functional details. Nuclear medicine brings out the functional details of the organ under study, but not the anatomical structures. Thus, they complement each other. Whereas, in echocardiography, both functional as well as anatomical details of the organ are available for study, which of course is another advantage of echocardiography.

### 1.1 BACKGROUND

A brief background in Clinical Cardiology will be appropriate at this point. When blood vessels have deposits of cholesterol, the effective volume of blood flow is reduced. There could be some structural impairment in the heart. In patients with rheumatic valvular heart disease, the leaflets of the affected valves become stiff damping their oscillations. This narrows the opening in the valves between chambers or between a chamber and a vessel depending on the valve affected. While ensuring the required amount of oxygen for the cells through such narrowed paths, the heart has to pump out blood at a higher rate as well as at a higher pressure. Because of these blockages, some amount of blood stays back in the ventricles during each cycle. This results



in a condition of hypertrophy or enlargement of the heart.

A temporary blockage in any of the coronary arteries would deprive a part of the heart muscles, served by that artery, of required oxygen. Because of this, that portion of the heart wall would fail to function normally. In general terms, this is called a heart attack. After a heart attack, the tissues involved are dead, a scar develops at that place and the elasticity of that portion of the heart walls is affected. When it occurs in the left ventricle, as it often does, it is called an infarction of the left ventricle. The result of this is bulging of the heart wall aggravated by higher pressures in the left ventricle. The distortion in shape is of particular importance as it is an indication of abnormal conditions.

There is a definite change in thickness of the heart walls between the extremes of two strokes: end-systole and end-diastole. If there is an abnormality in the structure of the blood vessels or valves or a change in the elasticity of the wall as described in the preceding paragraphs, the change in thickness of the left ventricular muscles and the amount of blood pumped out in a cardiac cycle will be significantly affected.

Several diseases associated with the cardiac system involve the size and shape of the heart and characteristics of the heart walls [Hab80, Mil82]. Hence, a study of the shape of the heart at different points in the cardiac cycle, the size of the individual chambers and the changes in the

wall thickness of the heart are important in order to diagnose and understand cardiovascular abnormalities. Once these abnormal phenomena are understood, many human lives could be saved through prompt action by cardiologists. It should also be reiterated that such a study should be carried out in a manner that is not by itself destructive. The necessity for non-destructive study of heart has been realized as early as 1971 in following the progression of disease in a natural way [Pom71].

It is possible to conduct the above-mentioned studies with ultrasonic imaging which is non-invasive and involves minimum discomfort to the patients. Instrumentation techniques help in the development of ultrasonic transducers that convert sound signals to electrical signals. An electronic interface connects such transducers to modern computers that are fast, reliable and accurate. Raw information, whatever the amount presented, is of little use unless it is processed in a definite context and presented in a form that is convenient for the user. Image processing techniques play a vital role in processing the information in these images while the displays act as an efficient man-machine interface. Digital image processing techniques have two major applications. They can be used to improve the image quality and thereby make it easier for the medical practitioner to perform analysis. Such preprocessing applications have been described in the literature [Led79, Hee79, Lee80, Hoh82]. They have also been considered for fully

automating the analysis of images in many areas, e.g., character recognition, finger prints, satellite images and medical images, etc. [Roe73]. Analysis of echocardiograms falls under the area of medical image processing. A procedure for enhancing echocardiograms with computers will be presented here.

## 1.2 SPECIFIC PROBLEMS

Imaging of the heart, however, is not as simple as may be first thought, i.e., it is in continuous motion and it is not easy to stop it for some time. Furthermore, the position of the heart keeps changing due to diaphragmatic movements, rendering consistent positioning difficult. The transducer angle, heart size and body position also play vital roles in image reproducibility [Won81].

The left ventricle of the heart supplies blood for every cell and hence energy for the whole body including the heart itself. Therefore, the left ventricle plays an important role in the well being of the body. The objectives of any echo-cardiographic study are:

1. To get the incremental volume/ejection fraction of the left ventricle (LV).
2. To get the left ventricular wall thickness at different places at different points of the cardiac cycle.
3. To study the left ventricular wall motion.

Major impeding factors are the inherent noise in the images and the difficulty in correlating the images due to heart motion in the chest cavity which is mainly because of respiration. For example, the images have both translational and rotational motion. Any automatic procedure to analyze echocardiograms should first focus on these problems and take measures to correct them. Looking at the specific problems listed above, it is apparent that the outline of the heart walls at a desired instant of time would be very useful. With the outlines at end-systolic and end-diastolic phases of the EKG, measurements can be easily made to compute the incremental volume and ejection fraction of the left ventricle. If the wall outlines can be found at different points of the cardiac cycle, thickness can be measured at different places of the heart wall. These outlines also show how the heart wall moves during a cardiac cycle. So, this thesis will concentrate on obtaining the outlines of the heart walls from the input images.

### 1.3 ORGANIZATION

In Chapter 2, the fundamentals of ultrasonic transducers, their application to cardiac imaging and different modes of imaging in practice are explained in brief.

Chapter 3 gives a survey and analysis of noise filtering methods. A noise filter that is based on a set of

neighboring pixels of almost uniform gray level, but not of any fixed size is proposed. Results of applying these filters to test images are given.

Chapter 4 presents several edge operators found in the literature. A new edge operator is proposed that is more suitable for the type of images encountered. The results of employing these operators on smoothed test images are also presented.

A survey of several contour tracing schemes is given in Chapter 5. It also contains a scheme that combines the important properties of two such algorithms and gives better results than those.

A discussion on the limitations and drawbacks of the proposed procedure such as open contours and manual interactions will form the conclusion of this thesis. A critical review of the proposed algorithms is given here. A few suggestions to overcome the limitations of this procedure also will be presented in the conclusion.

## CHAPTER 2

### ULTRASONIC ECHOCARDIOGRAPHY

Ultrasonic frequencies lie above the audible range of human ears whose upper limit is approximately 20 KHz. The application of ultrasonic echoes date back in history, as they were used for orientation, navigation and communication by mammals. Ultrasonic echoes were first observed in bats for sensing and navigation purposes. Then they started finding their application in several areas of science similar to those in nature. Experiments using ultrasonic echoes were later developed for measurements of ocean depth and submarine detection. Though ultrasonic echoes have been applied in biology and medicine only recently, the applications are remarkable and the diagnostic applications of ultrasound are very popular. This chapter will concentrate on ultrasonic transducers for imaging the heart and the different modes that are possible with such transducers. Interested readers may further refer to Hewlett-Packard Journals and similar materials [HPJ83, a]

#### 2.1 PHYSICS OF ULTRASONIC TRANSDUCERS

In ultrasonic transducers, there is a source which produces mechanical vibrations in the appropriate frequency

range and a receiver to detect the sound reflected from the object in the path. Transducers normally consist of piezoelectric crystals that convert electrical energy to mechanical energy and vice versa. A piezoelectric crystal is cut along a particular axis to a certain thickness. When this is subjected to an electric field, it undergoes a mechanical deformation along a predefined axis depending on the direction of the electric field. If the applied field is varied rapidly, the compression and expansion also varies at that rate. When the frequency of the electric field reaches the crystal's natural frequency, the crystal resonates. The amplitude of this vibration depends on the strength of the applied field. The natural frequency of the crystal is determined by its thickness; the thinner the crystal, the higher its resonant frequency. In the receiver, the opposite phenomenon takes place. The reflected sound waves are incident on a similar piezoelectric crystal and produce electrical signals.

Depending on the distance of the object, the echoes arrive at different times. The time taken to get the echo depends on the distance of the object from the source. The strength of the echo is determined by the medium. Different media absorb energy in different proportions and the absorption is directly proportional to the frequency of excitation. Scattering and divergence increase with distance and they cause attenuation of the energy received. When the sound travels from one medium to another of different

10

density, a part of the wavefront is reflected while the rest proceeds further. This brings in the concept of characteristic impedance that is defined as the product of the propagation velocity of sound in that medium and the density of the medium. The velocity of propagation depends only on the medium and not on the frequency of the sound wave. Hence, in a particular medium, the distance of the object can be easily calculated by measuring the time taken for the echo to reach the receiver from the time the sound wave is transmitted if the velocity is precisely known.

In practice, the transducer would have protection for its crystal to avoid photoexcitation ringing. The transducer also has backplates to absorb the wavefronts produced in directions other than that required. The sensitivity of the crystal is further increased by providing an external tank circuit. In some transducers, acoustic collimators are used to achieve a narrow beam which would facilitate observing small objects. The characteristics of the transducer used depend upon its use.

A transducer may contain a single or multiple crystals. In case of single crystal devices, the sound is transmitted periodically in brief pulses during which times the crystal acts as a transmitter and during the rest of the period it acts as a receiver converting the echoes. A typical set of operating characteristics of such a transducer used for adult hearts would be [a]:



Sonic frequency	2.24 MHz
Pulse repetition rate	1024 per sec
Transmission time	1 micro sec
Reception time	999 micro sec

The transducers may also have two crystals, one for transmission and other for reception. The receiver could get echoes from different boundaries at different times depending on the distance. Therefore the transmitter should be off until all the echoes die out after every burst of transmission to ensure that no overlapping echoes and hence no incorrect information is obtained. This involves duplication in hardware without any added advantage. So, these transducers are not generally preferred. Transducers with one or two elements as described above are called single beam transducers.

## 2.2 IMAGING MODES

Displays obtained with single beam transducers fall under three categories: Amplitude Mode (A-Mode), Brightness Mode (B-Mode) and Time Motion Mode (M-Mode). As mentioned earlier, the echo strength depends on the characteristics of the medium. Furthermore the time taken for the echo to arrive at the receiver is a measure of the distance of the object. When the echo strength is converted to a proportional amplitude of deflection of the spot and the

time directly calibrated for distance of the structure from the transducer on the display, it is called Amplitude Mode or in short an A-Mode display. Here, a constant intensity spot sweeps the screen the deflection along y-axis being proportional to the echo amplitude. Each frame of this display gives a snap shot of the structures. Multiple frames are needed to understand the movement of one point on the heart wall. Thus, this display mode does not provide much useful information to study the movement. The amplitude in A-Mode or the echo strength is converted to brightness of a spot in which case it is called Brightness Mode or a B-Mode display. This mode will give a line of dots of different intensity for each burst of ultrasound generated. By moving the spots on the screen at a constant rate, the movement of the structures can be recorded at each instant. This motion can be obtained either by moving the recording surface or the spot itself in a direction perpendicular to the direction of the distance axis. Thus the movement of the object could be studied along with the distance in this display mode. This mode is called Time Motion display mode or an M-Mode display.

### 2.3 LIMITATIONS OF SINGLE BEAM TRANSDUCERS

Sound reflected from obliquely held objects and from rough surfaces is greatly attenuated. Such echoes would mislead the user about the object. The echoes from two

different surfaces separated by half a wavelength of the transmitted sound or from some rough surface that would produce two such wavefronts would undergo destructive interference and hence would not be shown on the display. Depending on the frequency of operation there is a definite minimum distance of separation of objects for them to show up on the display.

The higher the frequency, the better the resolution but the beam penetration is less. In spite of the use of acoustic collimators to increase the penetration depth, the sound beam undergoes divergence after some distance. Wide beams cause superposition of objects that have lateral separation, that can be misleading in later analysis.

Due to the order of magnitude of echo strength from objects at different distances, the receiver amplifier has to be adjusted for gain with respect to time. This compression of amplitude range is accomplished in many practical transducers by using a time gain compensation technique.

Furthermore, single beam transducers cannot provide spatial information on moving objects. When they are applied to study moving heart walls, the distances between structures as displayed on the M-Mode echocardiograms only tell about the motion of the transducer and not about the cardiac structures. When the structural motion is not along the axis of the sound beam, the display is deceptive. The transducer is fixed at a point and a conical section of the heart is mapped onto a rectangular display; This angular relationship

further complicates the analysis.

While these transducers are useful in functional analysis they are very limited for use in structural analysis of the heart. The B-Mode scan could be used to get the cross section of the heart by triggering it with a point in EKG but this requires skill in recording and takes several cardiac cycles to complete one section. Displacement of the heart and irregular heart rates pose further problems in imaging.

#### 2.4 TWO DIMENSIONAL IMAGING

To circumvent most of these problems, two dimensional echocardiographic imaging systems that operate in real-time have been developed. Two dimensional imaging can be accomplished in several ways. The transducer is moved discretely and rapidly producing a wedge section of heart at every scan. The echoes are then electronically translated during display. Mechanical scanners can be replaced by a linear array of transducer elements triggered in a predetermined sequence and the display is formed by the echoes of each of these elements. A typical multi-element transducer consisting of 20 crystals will have an active surface of 1 cm width and 8 cm length. The format of the echoes and display are compatible for mapping one onto the other and the echoes are conveniently recorded on video tapes. When a transducer consists of an array of elements in

a cluster, by altering the sequence of firing of the individual elements, the additive effect of all these elements and hence the whole transducer angle could be changed [von76]. Figures 2.1, 2.2 and 2.3 illustrate this principle. For an illustration of the ultrasound beam, its coverage and the method of scanning the reader is referred to HPJ83. The fan of transducer elements thus sweep a cardiac cross section typically 20 times a second while still maintaining a resolution of 2-4 mm throughout the field of view. Figure 2.4 gives a cross section of the heart and the cone of view obtained by such a phased array transducer. This provides a very good quality image at the cost of sophisticated central programming to effect the sequence of firing.

The investigator, with this kind of two dimensional real-time cross-sectional imaging systems, has better visual feedback for positioning the transducer and for adjusting its gain control settings to get the required view in a short time. The data output is compatible for storage and processing and hence costs less. Generally, the data is stored on a videotape for later conversion to a digital format and use on digital computers. In this work the video tapes were played back and frames were grabbed and digitized on the fly by constantly observing the display. The frame digitized in this manner may be different from the one intended. So, the process is repeated until the digitized frame is very near to the one actually needed. This error

cannot be avoided because there is no facility currently available to grab frames of interest such as triggering with a point on EKG.

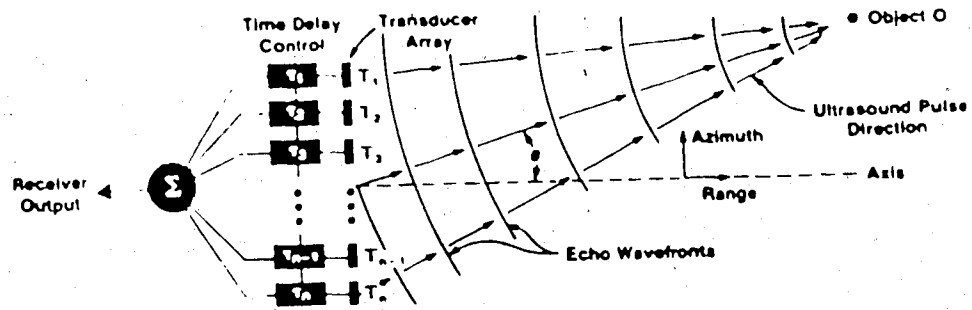


Figure 2.1 Block diagram of phased-array system

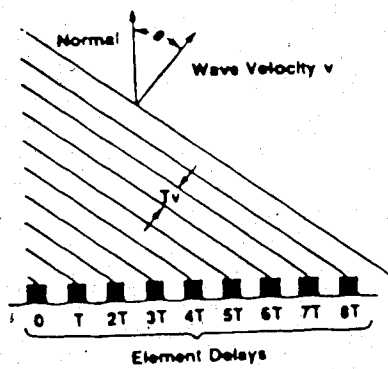


Figure 2.2 Phased array radiating a plane wave at an angle  $\theta$ .

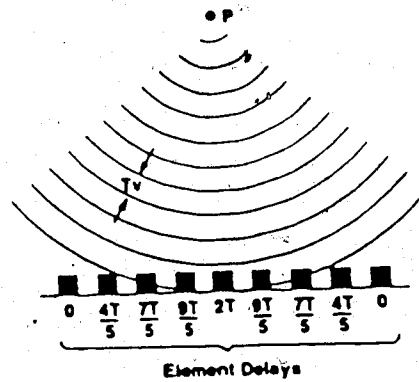


Figure 2.3 Phased array radiating a wave focused at point P.

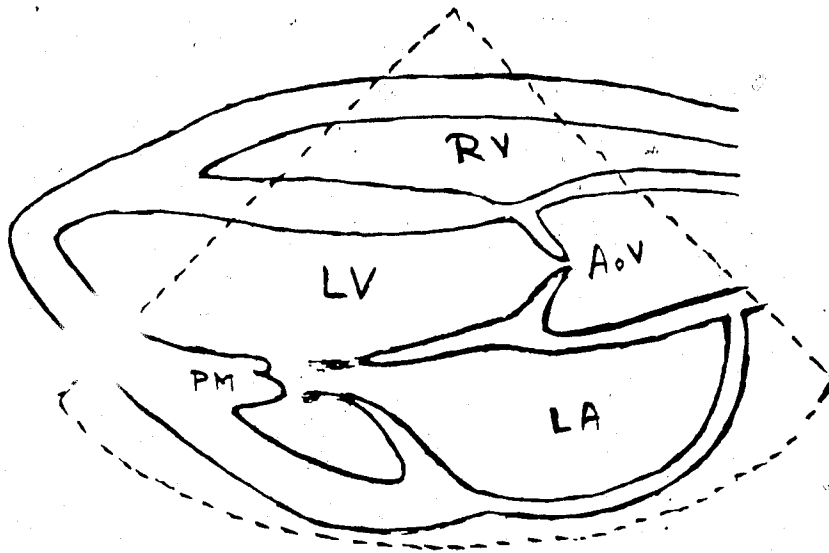


Fig. 2.4 A cross section of the heart. Dotted cone is the view obtained by the transducer.

## CHAPTER 3

### NOISE FILTERING

A digital image essentially consists of intensity levels at various sampled points of the picture. An element of such a digital image is termed a picture element or in short *Pixel*. The range of values used to represent a pixel depends on the number of bits used. For example, if eight bits were used for a pixel, 256 distinct intensity levels of the picture could be represented. As is evident at this point, the digital image of a picture is not an exact representation of the picture; it is influenced by sampling and quantization errors. The larger the number of *bits* used to represent a *pixel*, the less the *quantization* error and the larger the number of *pixels* used to represent a *picture*, the less the *sampling* error. But the result of reduction of such errors is an increase in the amount of storage required to represent a picture. Generally, an attempt is made to choose optimum values for representing an image. The effect of equipment and other environmental factors still exists which will introduce noise in digitized images.



### 3.1 EXISTING METHODS

Several techniques [Ros76, Gon77, Pav82] can be found in the literature to remove noise in digital images. No single technique is applicable to all classes of images. They are to be studied for choosing the most suitable one for our purposes.

Bandpass filters, that employ frequency thresholds as a measure, applied in cascade or a double bandpass filter give good results [Pöp82] for images where contours are critical. This method is computationally costly as it operates on the Fourier Transformed image in the frequency domain. Hence, most of the techniques operate in the spatial domain.

If the observed values of the pixel gray level at any point  $(x,y)$  is  $O_{xy}$ , it has contributions from:

1. actual signal value  $S_{xy}$  that only has the information and
2.  $N_{xy}$  the noise due to the equipment, the environment and the like.

i.e.,

$$O_{xy} = S_{xy} + N_{xy}. \quad (3.1)$$

Suppose a subset  $P$  of the image consisting of the pixels around the point  $x, y$  is taken and a *measure* of observed intensity level over this set is  $M(P)$ . Then, the error involved in taking this value for the signal intensity

at the point under consideration would be

$$E_{xy} = | S_{xy} - M(P) |. \quad (3.2)$$

Any preprocessing algorithm should aim at minimizing this objective function.

Averaging with weights dependent on local mean and variance has been considered as a measure for noise filtering in a technique developed by Lee and it does not require any transforms [Lee80]. The method proposed by Tomita et. al. [Tom77] has been improved [Nag79] with nine different masks. This assigns the average gray level of the mask region that has least variance to the pixel under consideration. i. e., the most uniform neighborhood area of a point is chosen and the average gray level of this region is assigned to the point. This technique is claimed to preserve edges and contours while removing noise in the image.

Linear models for the underlying image and the superimposed noise require prior knowledge of the characteristics of the image and they usually result in edge distortions. Some methods involve non-linear models for the image and noise to restore the original image. Consequently, they are not very easy to analyze. Non-linear techniques involving local operations such as mean and median also have models for noise reduction; but the assumptions implicit in these techniques are more general than those needed by optimal linear filter approaches. These non-linear methods

try to retain the important features in the image such as edges while reducing the noise content. Also, as these techniques do not require any *a priori* knowledge of the images, they are easier to implement. Their multiple and/or repetitive applications tend to improve the image quality. Chin and Yeh present an evaluation of several of these methods [Chi83]. The following techniques will be considered in this research for noise reduction:

1. Median filters
2. Unweighted averaging over 3 x 3 neighborhood
3. Unweighted averaging over 5 x 5 neighborhood
4. Smoothing with weights dependent on spatial distribution of the neighboring pixels in a 3 x 3 region
5. Smoothing with weights dependent on gray level distribution of the neighbors in a similar region
6. Smoothing with weights dependent on both spatial and gray level distributions of the neighbors.

### 3.2 EXTRACTION OF REGION OF INTEREST

The digitized frames have other patient information recorded on them such as the EKG which is not relevant to the image operations. Plate 3.1 is such a frame that also exemplifies the quality of the image that is received for processing. Since only the portion of the image with the ventricle is of interest, that portion is extracted from the image. Essentially, this process reduces the amount of data



Plate 3.1 Original echocardiogram of frame 1

to be processed and lets further processing concentrate only on the relevant data. The extraction itself is done interactively by pointing to the approximate center of the region of interest (ROI), with the help of a cursor and a tablet or in the absence of a tablet with a cursor and a keypad. A picture matrix of size 256 x 256, with this point as the center, is read out. Such picture matrices are used as input to various filtering algorithms for comparing those algorithms. During the process of extraction itself the data can be smoothed by employing any of the methods that follow. Plate 3.2 is the ROI of the frame shown in Plate 3.1. Plate 3.3 is extracted from another frame, the original frame of which is not shown here.

### 3.3 MEDIAN FILTER

The *measure* of the observed intensity levels used for noise removal in median filters is the median of the neighboring pixel values. Consider a neighborhood of size  $n \times n$  such that the point under consideration is at the center. Then, if the pixel values in this neighborhood points are arranged in a monotonically increasing sequence, the median of this sequence, i.e. the value at the position  $(n^2 + 1)/2$  would be an approximation to the signal value at this point. Essentially, this examines the trend of the intensity at different points over a small region for the

1 When 'n' is even the position considered can be either  $n^2/2$  or  $n^2/2 + 1$ .



Plate 3.2 ROI in echocardiogram - frame 1



Plate 3.3 ROI in echocardiogram - frame 2

probable gray level at the center. Plates 3.4 and 3.5 show the results of median filtering the originals given in Plates 3.2 & 3.3 respectively. The histograms are also superimposed on the images. Experiments [Pöp82] reveal that median filters do not work well for objects with noisy contours where preservation of the contour is important for later analysis.

### 3.4 AVERAGING

Another measure could be the average value of pixels of the neighborhood  $P$  considered before. Looking at the objective function given by (3.2), two things become obvious.

1. The neighborhood chosen should be small. Otherwise, the information contained in small regions is lost. It should be just sufficient to eliminate the spatial frequency noise.
2. Averaging should be such that the absolute difference between  $M(P)$  and  $S_{x,y}$  is as small as possible for all  $(x,y)$  in the chosen neighborhood.

The trivial neighborhood to satisfy these criteria is the degenerate single pixel with null neighborhood. The next one that also retains symmetry would be a 3 x 3 matrix with the pixel under consideration at its center. Larger neighborhoods of 5 x 5 or 7 x 7 matrices can be looked into. But the size of the neighborhood is subject to the



Plate 3.4 Median filter output for frame 1



Plate 3.5 Median filter output for frame 2



consideration of the size of the image, background illumination and contrast levels in the image. The size is also mainly constrained by the first observation above.

### 3.4.1 Unweighted Averaging

This is probably the simplest filter any one could think of and is described in every textbook. If  $F(x,y)$  is the given  $N \times N$  noisy image, the gray level at every  $(x,y)$  in the smoothed  $N \times N$  image  $F'(x,y)$  is obtained by averaging the gray levels of a predefined neighborhood  $P$  of  $(x,y)$  in the noisy image. It can be expressed by the following equation:

$$F'(x,y) = [\sum F(a,b)] / S. \quad (3.3)$$

where,  $a$  and  $b$  range over the chosen neighborhood  $P$  and  $S$  is the total number of pixels in  $P$ .

The unweighted average over the neighborhood of  $P$  suffers from two major disadvantages.

1. If the image has high contrast regions, it loses those small regions.
2. When the scene has individual pixels whose gray level is considerably different from its neighbors, the second requirement mentioned earlier in this section will not be met.

The size of the regions lost depends on the neighborhood size chosen for averaging. A larger  $P$  will lose larger regions. When applied to multimodal images in which the gray

levels belong to several distinct groups separated by a wide gap of intensity levels, the unweighted averaging smooths these variations. As sharp edges are blurred, further processing depending on edge information will not give good results. Hence, it is clear that unweighted averaging is not suitable for most applications that depend on minute edges. The results of unweighted averaging performed on images of Plates 3.2 & 3.3 over 3 x 3 neighborhood are given in Plates 3.6 & 3.7 respectively. Plates 3.8 & 3.9 are the corresponding outputs of unweighted averaging over a 5 x 5 neighborhood without assigned weights. It is seen clearly in these plates that the latter two images are more diffused than the former ones because of larger neighborhood size considered.

### 3.4.2 Weighted Averaging

Weights could be assigned to each of the neighboring pixels to prevent the loss of edges. Weights can depend either on spatial separation or on the gray level difference between the pixel under consideration and its neighbors, or both.

#### 3.4.2.1 Spatial Weights

The farther apart the neighbors, the less should be their effect on the pixel under consideration. Davis and Orthner [Dav79] have considered several weight



Plate 3.6 3 x 3 unweighted averaging output for frame 1



Plate 3.7 3 x 3 unweighted averaging output for frame 2



Plate 3.8 Output of 5 x 5 unweighted averaging on frame 1

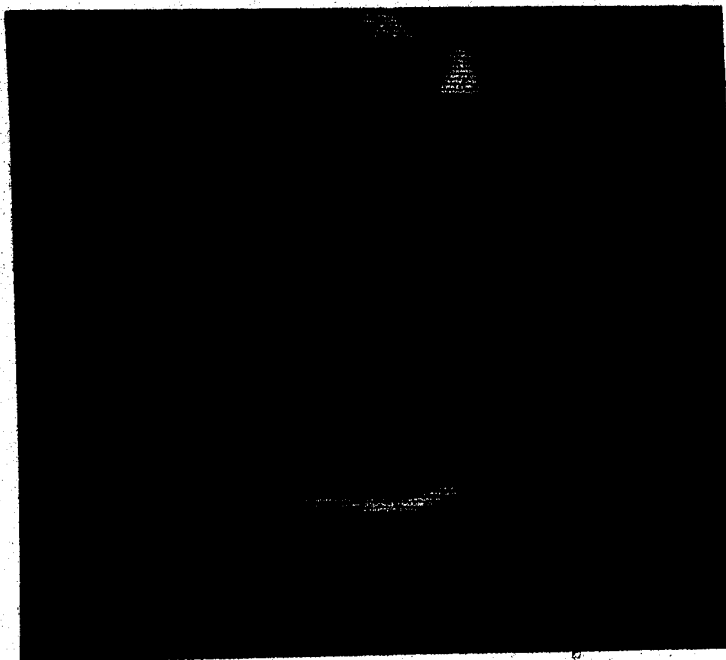


Plate 3.9 Output of 5 x 5 unweighted averaging on frame 2

assignments. Weights proportional to  $X-d$ ,  $X/d$ ,  $X/(d+1)$  and  $X/(2d+1)$  were assigned to the neighbors where  $X$  is an arbitrary weight of  $2(S+1)$  assigned to the center pixel and  $d$  is the manhattan distance of the pixel from the center. The performance was studied over  $3 \times 3$ ,  $7 \times 7$  and  $11 \times 11$  matrices. It was found that

1. the larger the neighborhood used the more the boundaries become smoothed with the disappearance of small regions.
2. the less the weights are concentrated at the center the more continuous the boundaries are.

Here, the weights assigned to neighbors are inversely proportional to the square of the distance. For the neighborhood:

a	b	c
d	e	f
g	h	k

$$F'(e) = \{ [F(a) + F(c) + F(g) + F(k)]/2 + (F(b) + F(d) + F(f) + F(h)) \} / 8.$$

$$M(P) = F(e) \quad \text{if} \quad |F'(e) - F(e)| < TH,$$

a nonnegative threshold.

$$= F'(e) \quad \text{otherwise.}$$

(3.4)

Where,  $F(e)$  is the gray level at point  $e$  in the

original image and  $F'(e)$  is the gray level at the same point in the filtered image. Thus, the effect of distance of neighboring points on the gray level at a point is considered and thresholding helps reduce blurring. Indirectly, this filter conforms to the observation on neighborhood size. The contribution to gross error due to neighborhood effect is minimized to a great extent. Here, the threshold is set to 8, i.e., only if the modified gray level differs more than 8 from the gray level in the original image will it be changed. Plates 3.10 & 3.11 are the results of such averaging done on Plates 3.2 & 3.3.

It is apparent in the equation 3.4 that the contribution by the axial pixels are less than what they really should be. The constant divisor should have been 6 instead of 8 to correct this error.

#### 3.4.2.2 Gray Level Weighting

When a neighboring point is very different in its intensity level from the point under consideration, unweighted averaging changes the gray level of the latter. As the regions of non-uniform gray levels are merged together during such changes, unweighted averaging loses edge details in the image. This loss can be avoided if the neighbors are assigned weights depending



Plate 3.10 Spatial weighted filter output for frame 1



Plate 3.11 Spatial weighted filter output for frame 2



Plate 3.12 Gray level weighted filter output for frame 1



Plate 3.13 Gray level weighted filter output for frame 2



on the gray level difference. The more a neighboring point is different in its intensity level the less its contribution on changing the point under consideration. Effectively, this scheme concentrates on calculating a measure from a uniform region of the neighborhood rather than the whole of it. This has been studied by considering regular geometric regions around a point [Tom77, Nag79]. The latter referenced study, an improvement over the former, considered nine different bar masks as shown in Figure 3.1.



Figure 3.1 Averaging masks

The average gray level of the mask region that has the least variance to the gray level of the point under consideration is assigned to that point. It can be seen, then, that this method considers edge formation only in certain predefined orientations and shapes. Here, that method is improved by considering any

arbitrarily shaped mask that will align best with the edge in the neighborhood. A predefined number of points in the neighborhood is taken that differ least in their gray levels from that of the point under consideration. If their average is assigned to the point under consideration, the mask is allowed to take any arbitrary shape that aligns with the shape of the edge in that neighborhood. 5 pixels out of 8 neighbors in a 3 x 3 matrix with the point under consideration at the center of the matrix are taken for averaging. This gives 56 masks of different shapes out of which the one that best aligns with the local edge is taken for averaging. A weight of 1 is assigned to those pixels that differ least in their gray levels from that of the center and a 0 to others. This technique should give better results in the form of edge preservation than that described in [Nag79] and certainly better than unweighted averaging. The number of pixels considered for averaging will affect the results in different quality images. When the picture is busy fewer neighbors should be taken for averaging. Application of this scheme on images on Plates 3.2 & 3.3, gives outputs as shown in Plates 3.12 & 3.13.

#### 3.4.2.3 Double Weighted Smoothing

Combining the two aforesaid ideas, one could attempt to assign weights to the neighborhood points in terms of

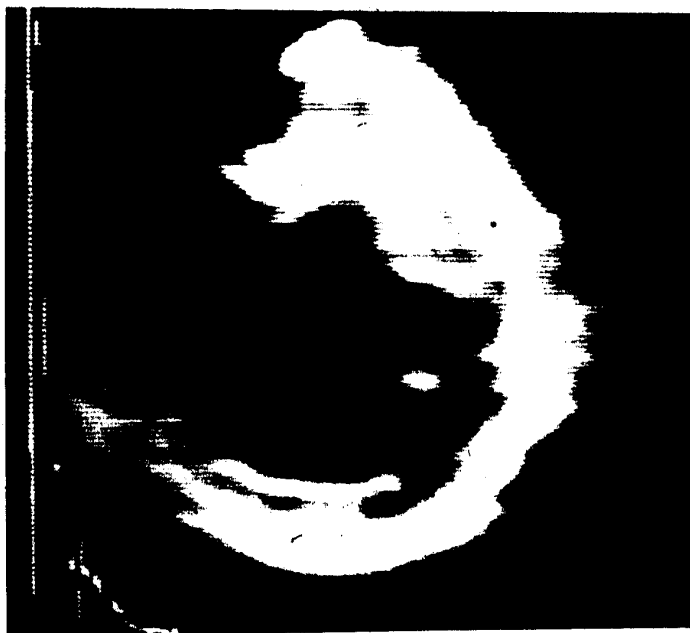


Plate 3.14 Output of filter with both weights - frame 1



Plate 3.15 Output of filter with both weights - frame 2

their difference in intensity levels and distance. This scheme would incorporate central pixel dominance in terms of spatial as well as gray level separations. An algorithm based on this is found in the literature [Ove79] which is suitable for cleaning noise from busy pictures.

The observed gray level  $O(x)$  is modified to  $O'(x)$  as

$$O'(x) = \frac{O(x) + \sum_{j \in N} Ws(j,x) \cdot Wg(j,x) \cdot O(j)}{1 + \sum_{j \in N} Ws(j,x) \cdot Wg(j,x)} \quad (3.5)$$

where,  $Ws(j,x)$  is the compensation for spatial separation of the neighborhood pixel at  $j$  from the point under consideration and it is given as

$$Ws^2(j,x) = \frac{1}{[R(j)-R(x)]^2 + [C(j)-C(x)]^2} \quad (3.6)$$

$R(j)$  and  $C(j)$  are the row and column values of the pixel at  $j$ . It is evident here that the diagonal pixels have lesser weight than the axial ones due their distances.

$Wg(j,x)$  is the weighting function for gray level separation of the pixels from that of the pixel under consideration and the function is expressed as follows:

$$Wg(j, x) = \frac{1}{1 + |O(j) - O(x)|^{Pjx}} \quad (3.7)$$

$$Pjx = |O(j) - O(x)|^2 / V \quad (3.8)$$

The power function in (3.7) is very critical and has been chosen by [Ove 79] after studies as given in (3.8).  $V$  is the statistical variance though factors like standard deviation would work equally well for this. The images given on Plates 3.14 and 3.15 are the results of employing this double weighted averaging scheme for images given on Plates 3.2 and 3.3 respectively.

### 3.5 COMPARISON OF RESULTS

All these filtering schemes were implemented (see Appendix A) and the following table gives their performance on a typical image of size 256 x 256.

Table 3.1

## Comparison of Noise Filters

Mean Gray level of the original of size 256 x 256 is 51

Filter	Elapsed time in secs	Mean	% change in mean	Mean Square Error
Unweighted 3 x 3	14.417	51	0.004	8.6049
Unweighted 5 x 5	23.0	50	0.008	17.887
Spatial Weights*	26.784	53	0.023	77.630
Gray Level Weights*	156.167	50	0.011	28.261
Double weights*	1472.817	50	0.005	0.681
Median*	180.0	51	0.003	16.806

\*over 3 x 3 neighborhood.

### 3.6 CONCLUSION

Unweighted averaging is the fastest of all these but has a tendency to blur the edges of regions. So, if the picture contains minute edges of interest for later use, then this method is not suitable for such applications. The size of regions lost by blurring depends upon the neighborhood size chosen for averaging. Generally, the neighborhood chosen is 3 x 3 or 5 x 5 if symmetry is to be retained. For larger pictures bigger neighborhoods can be considered.

For obtaining the heart wall boundaries in echocardiograms, the gross pattern of the cross section is of interest and not minute structural details. The weighted averaging schemes will detect minute details. These details would clutter the image and make later processing steps tedious. In the present application, the characteristic of diffusing tiny edges in the image by the unweighted averaging technique and the speed of the algorithm to process images are taken advantage of. The outputs of all aforesaid filters were also considered for further processing of edge detection and contour tracing and the results compared for establishing this conclusion.

## CHAPTER 4

### EDGE DETECTION

An image can be segmented into regions by simply thresholding it; the threshold being dictated by the gray level histogram of the image. This approach gives good results for converting a gray level image to a binary image in fingerprint processing applications [Ven77]. The resulting binary image meets the desired fidelity standards after a couple of preprocessing steps. Thresholding alone has been considered for segmentation of echocardiograms [Sko81], but not with great success. The ventricular border varies significantly with the threshold chosen. In multimodal images the choice of threshold is difficult as the threshold tends to be localized. Several boundaries need to be generated if there is more than one minimum in the gray level histogram of the image. Local thresholds become prohibitively expensive for large images. For an improvement in segmentation, edges can be detected in the image which assist in region growing. When the intensity level in an image undergoes sharp changes, edges are formed. Edges can be resolved if the gradients at all points of the image are calculated continuously.

An edge operator should have its response

1. independent of the edge orientation and



2. fall sharply as it is moved away from the actual location of the edge.

Many edge operators exist; however, their performance varies over a wide range. The performance also depends, to some extent, on the image characteristics. Some of the edge operators found in the literature [Nev82, Pel82] are given here. Wherever possible, the existing operator is modified and extended to rectify the drawbacks inherent in that operator. Sections 4.7, 4.8 and 4.10 are the outcomes of such modifications.

#### 4.1 IMAGE COMPRESSION

It has been shown that by shrinking a digital image and then expanding it helps to remove noise near the edges [Ros76]. A strategy similar to pyramid encoding is adopted here for shrinking the image and thus to ultimately remove noise near the edges. The gray levels in every  $2 \times 2$  neighborhood of the smoothed image are averaged and the average becomes the gray value in a new image. This step compresses the  $256 \times 256$  image into a  $128 \times 128$  image and during that process smooths the noise near the edges. The reduction in size is an added advantage because it reduces the amount of data for further processing. In Plate 4.1a, the compressed form of the image on Plate 3.2 is presented.

## 4.2 HISTOGRAM STRETCHING

Because of the poor contrast in the images, it is useful to alter some of the gray values. The histogram of the compressed image is calculated, and a transformation is determined so that the gray values are more evenly distributed over the full range. Contrast stretching the images not only improves the visual appearance, but also results in fewer discontinuities in the contours produced by the edge operators.

Supposing the gray level at the lower end of the scale with a significant number of pixels (0.03% area of the image) is 26 and the bright area of reasonable size (same as before) is 111 - this is a typical range and is the case for the image in Frame 1. Then, the gray levels in the range of [26,111] is linearly mapped onto the full range [0,255]. The gray levels in [0,25] are converted to 0 and those in the range [112,255] are converted to 255. Thus, it stretches only the gray scale in the range that has information and compresses in the other ranges. This avoids smearing of contours and discontinuities because of false edges. Also as the gray levels of the range of interest are enhanced, the edge values are increased by a factor which will be helpful in contour tracing. Plate 4.1b is the result of histogram stretching the image on Plate 4.1a. In comparison to Plate 4.1a, clarity in details can be noticed in this image.



Plate 4.1 Frame 1 is (a) Compressed (b) Histogram stretched

### 4.3 SECOND LEVEL SMOOTHING

Contrast stretching has introduced some problems while correcting others. It requires multiplication of the gray levels by a factor which need not be an integer. In fact, as it turns out, most of the time it is associated with an integral fraction. The modified gray levels will then be mapped into a discrete scale. This is a forced approximation of the gray levels for the modified pixels to their nearest integral values. Not only does this introduce quantization noise, but it may also omit some integral values. These discontinuities should be removed before further processing. Unweighted averaging over a 5 x 5 neighborhood is used at this stage for solving this problem.

### 4.4 GRADIENT ALGORITHMS

The simplest way to detect edges is to find the gradient at every point and then threshold the gradient values [Gon82]. If  $F(x,y)$  represents the picture at a point  $(x,y)$  and  $G(x,y)$  is the pixel value in the gradient image at the corresponding point,

$$G(x,y) = T F(x,y) \quad (4.1)$$

The general form of  $T$ , the transfer function, would be given as

$$T = A + B\nabla^2 \quad (4.2)$$

where  $A$  and  $B$  are constants and  $\nabla^2$  is the Laplacian operator and is given as

$$\nabla^2 = \delta^2/\delta x^2 + \delta^2/\delta y^2 \quad (4.3)$$

In its simplest form, the transfer function  $T$  can be written as

$$T = B^2 |\nabla^2| \quad (4.4)$$

With (4.1) and (4.4), the edge merit at a point  $(x,y)$  is given by

$$|(\delta F/\delta x)^2 + (\delta F/\delta y)^2| \quad (4.5)$$

Because this is the square of absolute magnitude of the gradient vector, it is invariant under translation and rotation. When applied to digital pictures, the derivatives are replaced by difference operators. The edges found by this operator will be split into two at each transition where only one edge is desired. Therefore, Laplacians are not very good for smoothly blurred edges.

#### 4.5 THE ROBERTS OPERATOR

The Roberts operator [Ros76] considers the neighborhood of four points given by

$$\begin{array}{cc} i,j & i+1,j \\ i,j+1 & i+1,j+1 \end{array}$$

If the gray value of the image at the point  $(i,j)$  is  $F(i,j)$ , this operator approximates the gradient by

$$\max \{|F(i,j)-F(i+1,j+1)|, |F(i,j+1)-F(i+1,j)|\} \quad (4.6)$$

As the differences are symmetrical about the point  $(i +$

$1/2, j + 1/2$ ); the edge value assigned is for that location. Although the Roberts operator locates edges in correct position (i.e., it satisfies the second criterion very well) it is highly direction and noise sensitive [Pel82]. Its application results in discontinuities in the boundaries traced. Also, this operator is reported not to work well for images with very gradual intensity variations [Pöp82].

#### 4.6 BEST-FIT EDGE OPERATOR

Rosenfeld proposed the best-fit edge operator [Ros76] by fitting a minimum error plane to the gray levels in a  $2 \times 2$  neighborhood. A plane  $z = ax + by + c$  ( $a$ ,  $b$  and  $c$  are derived in [Ros76]) is fitted to the image neighborhood as shown in Section 4.5. Then,  $a$  gives the component of the gradient in the  $x$ -direction and  $b$  gives that in the  $y$ -direction. The edge merits can then be written as follows:

$$E_o = \{F(i+1, j) + F(i+1, j+1)\} / 2 - \{F(i, j) + F(i, j+1)\} / 2 \quad (4.7)$$

$$E_{90} = \{F(i, j) + F(i+1, j)\} / 2 - \{F(i, j+1) + F(i+1, j+1)\} / 2 \quad (4.8)$$

where,  $\sqrt{E_o^2 + E_{90}^2}$  is the magnitude of the gradient at the center of this region. i.e.,  $(i+1/2, j+1/2)$ . This could be further approximated by  $|E_o| + |E_{90}|$  or  $\max\{|E_o|, |E_{90}|\}$ . (In this and all other subsequent operators, the last choice

is made for the magnitude of the gradient values.) This operator detects the edges of texture boundaries as well. The operator averages the pixels over a very small area before computing the gradient and hence it is less sensitive to noise. It is also biased towards edges oriented along the co-ordinate axes of the neighborhood similar to many other operators. It uses only a part of the immediate neighborhood for averaging. Hence, though the noise in one sector of its neighborhood is smoothed that in other sectors may still influence the gradient.

#### 4.7 EXTENDED BEST-FIT EDGE OPERATOR

Rosenfeld's best-fit edge operator can be extended by considering a  $3 \times 3$  neighborhood instead of a  $2 \times 2$  neighborhood. The desirable property of local smoothing in the best-fit operator is incorporated in this extension to find the edges amidst noise. At the same time this operator is symmetric about the center of the neighborhood. This operator finds the local unweighted average of row/column for use in the gradient computations. Now, the neighborhood becomes:

a	b	c
d	e	f
g	h	k

Edge merits in two orthogonal directions are then expressed as

$$E_o = [\{F(c)+F(f)+F(k)\}/3] - [\{F(a)+F(d)+F(g)\}/3] \quad (4.9)$$

$$E_{90} = [\{F(a)+F(b)+F(c)\}/3] - [\{F(g)+F(h)+F(k)\}/3] \quad (4.10)$$

Because this operator does unweighted averaging over the neighboring pixels it has the undesirable effect of local blurring as discussed earlier.

#### 4.8 WEIGHTED OPERATOR OVER 3 x 3 NEIGHBORHOOD

The blurring effects of the earlier operator can be minimized by assigning weights to the neighbors. By enhancing the gradients with weighting functions, high contrast edges can be obtained. The operator mentioned in the preceding section is modified by assigning weights to the neighboring pixels inversely proportional to their distance from the center.



$$E_o = [F(f) + \{F(c) + F(k)\} / \sqrt{2}] - [F(d) + \{F(a) + F(g)\} / \sqrt{2}] \quad (4.11)$$

$$E_{90} = [F(b) + \{F(a) + F(c)\} / \sqrt{2}] - [F(h) + \{F(g) + F(k)\} / \sqrt{2}] \quad (4.12)$$

Though the results of employing this operator on test images are not shown here, they are better than those obtained with the earlier operator. Edges found by this operator are still weak and depend on the threshold selected. If the threshold is set too low, the number of edge elements obtained is too large although those elements are not of much use in the succeeding steps. If the threshold is set high, there are too many broken edges that make it difficult to obtain continuous contours.

#### 4.9 ELECTROSTATIC CHARGE ANALOGY

Sethi [Set82] proposed an operator over a 3 x 3 neighborhood with weights assigned to the neighbors. This operator is essentially a modification of the operator discussed in the previous section. The weights assigned to the neighbors in the last section have been modified. The gradient at the center of a 3 x 3 neighborhood can be thought to be equivalent to the electrostatic potential at that point due to charges at the neighboring points. The value of the charges are considered equal to the gray level

value at those points. Then, the weights are inversely proportional to the square of the distance. Contributions to the field intensity at the center of this neighborhood by the charges at other places in the neighborhood are summed as vectors to give the resultant field strength at that point. The components of the gradient in two axial directions would then be given by:

$$E_o \cong [F(f)+\{F(c)+F(k)\}/3] - [F(d)+\{F(a)+F(g)\}/3] \quad (4.13)$$

$$E_{90} \cong [F(b)+\{F(a)+F(c)\}/3] - [F(h)+\{F(g)+F(k)\}/3] \quad (4.14)$$

The approximation of the denominators by integers is to hasten the computation at a cost of about a 7% error. The use of this operator for the images on Plates 3.6 and 3.7 gives the results as shown in Plates 4.2 and 4.3 respectively.

#### 4.10 EXTENSION OF THE ABOVE OPERATOR

The operator described above is certainly a better choice among all those operators dealt with until now. But, as it is apparent, while that operator detects the edges oriented in axial directions very well, it loses edges oriented diagonally while thresholding. The edges aligned



Plate 4.2 Output of Sethi's operator for frame 1



Plate 4.3 Output of Sethi's operator for frame 2

with the diagonals are weakened while resolving them into their components along the axes. During thresholding, there are chances for these weak edges to be omitted from the gradient image. This effect may not pose serious problems when the interest is in finding the shapes in an image whose faces are aligned more closely with the regular axes. In echocardiograms where the interest is in finding shapes that are more circular, the weakening effect will cause discontinuities in edges. These discontinuities will make contour tracing difficult. Hence, it is only appropriate to attempt to detect edges that are oriented along other directions also. Then it will leave the components of the contour in all orientations intact even after thresholding.

Weight assignments being the same as in the earlier operator, the field strength at the center point is calculated in all eight directions instead of four. Gradients in two diametrically opposite directions are absorbed in one orientation. Then, the four components of an edge are given by the following equalities.

$$E_0 \cong [F(f) + \{F(c) + F(k)\}/3] - [F(d) + \{F(a) + F(g)\}/3] \quad (4.15)$$

$$E_{45} \cong [\{F(c)/3\} + F(b) + F(f)] - [\{F(g)/3\} + F(d) + F(h)] \quad (4.16)$$

$$E_{90} \cong [F(b) + \{F(a) + F(c)\}/3] - [F(h) + \{F(g) + F(k)\}/3] \quad (4.17)$$

$$E_{135} \cong [\{F(a)/3\} + F(b) + F(d)] - [\{F(k)/3\} + F(h) + F(f)] \quad (4.18)$$

They represent the magnitudes of the gradients in all eight directions around a point under consideration. Absolute values of these components are considered for choosing the maximum gradient at this point. When this operator is employed for edge detection in images on Plates 3.6 and 3.7, the resulting images are given on Plates 4.4 and 4.5.

#### 4.11 COMPARISON AND CONCLUSION

Two postprocessing steps for the smoothed images were described. Apart from smoothing noise near the edges they help in data reduction for subsequent steps and also provide better contrast. Several edge operators popularly found in the literature were implemented. The best-fit edge operator and its extension to 3 x 3 neighborhood give very weak edges. The weighted edge operator over this neighborhood is better than the earlier ones considered without weights; but still does not result in very strong edges. Sethi's operator

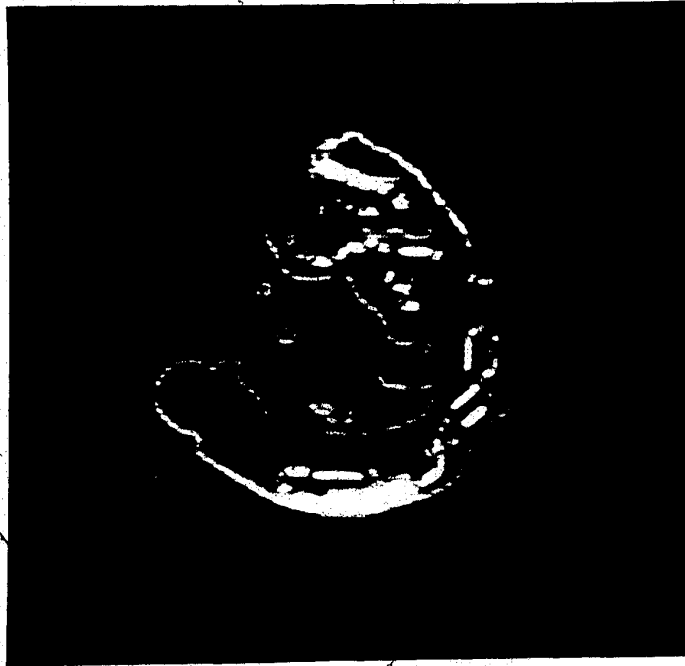


Plate 4.4 New operator output for frame 1

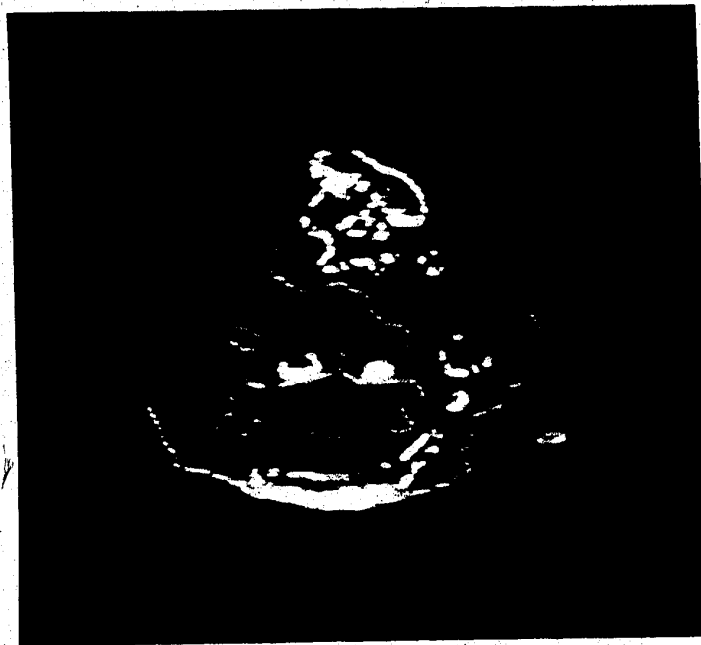


Plate 4.5 New operator output for frame 2

gives strong edges, but the output has more broken edges that make contour tracing difficult.

Thresholding is done in terms of the number of edge points rather than the gray level of the gradient. This eliminates the influence of the fixed absolute thresholds on different quality pictures where brightness and contrast affect the gradient values. Only about 10% to 15% of the image area is considered to have detectable edges. Hence, the histogram of the gradients is computed and thresholding is done as follows: The histogram of the edge image is calculated and the gray level that divides the histogram to the given percentage from the brighter end is found. This gray value sets the threshold, and the edges with brightness below this value are set to 0. The other edges are *not* assigned maximum values because their gray levels representing the gradients at these points are required later for contour tracing. At this threshold level the edges found by Sethi's operator are broken (mostly the diagonal edges) and they result in a discontinuous contour. The gradients output by Sethi's operator can be made to give continuous edges by increasing the threshold. However, raising the threshold has an obvious increase in the number of edge points that are to be considered by the contour tracing algorithms. It has been found by comparison that while about 18% of the image area is to be retained as edges in Sethi's gradient image, only about 12% of the image area is to be retained in the new extension for obtaining continuous contours. The traced

contours on frames 1 & 2 are presented in a later chapter as Plates 5.1 and 5.2, for subjective comparison of these edge operators.

Comparing the performance of all the operators considered, the operator mentioned last seems to be a refinement over all the others. During the study in [Set82] it has been found that the response of Sethi's operator is constant over a fairly wide interval of orientations and its sensitivity falls sharply after a small displacement of vertical edges. Different neighborhood sizes were considered and the performance of the operator for those neighborhoods have been compared [Set82]. As the proposed operator is an extension of this operator, it can be believed that those properties hold for this also, although no quantitative measurements have been made. This new edge operator seems to meet the requirements in producing a quality output for the echocardiograms, in terms of the contour.

However, the proposed new edge operator can be shown, on analysis, to be biased towards diagonal edges. Assume a constant change in gray levels in all directions from a point. In each of the equations 4.15 through 4.18, the first term is similar to the second. So, looking at the first term alone,  $E_0$  and  $E_{90}$  will be equal to 1.6 times the change in gray level if actual constants are used before rounding. Whereas,  $E_{45}$  and  $E_{135}$  will be equal to 2.3 times the change. Even if the electrostatic forces were resolved correctly, the latter will be equal to 1.9 times



the change. Only the maximum of these components is taken as the edge merit in the implementation of this operator.

Because the diagonal edges are amplified in comparison to the axial edges, weak edges having diagonal orientation are chosen in preference to the strong edges in axial direction. This may be the reason why the edges found by this operator are diagonally sliced at various places. In order to correct these errors, the equations 4.15 through 4.18 should be modified as suggested by Dr. Aoki [Aok84] and are rewritten as follows:

$$E_{0} = [F(f) + \{F(c) + F(k)\} / \sqrt{2}] - [F(d) + \{F(a) + F(g)\} / \sqrt{2}] \quad (4.19)$$

$$E_{45} = [F(c) / 2 + \{F(b) + F(f)\} / \sqrt{2}] - [F(g) / 2 + \{F(d) + F(h)\} / \sqrt{2}] \quad (4.20)$$

$$E_{90} = [F(b) + \{F(a) + F(c)\} / \sqrt{2}] - [F(h) + \{F(g) + F(k)\} / \sqrt{2}] \quad (4.21)$$

$$E_{135} = [F(a) / 2 + \{F(b) + F(d)\} / \sqrt{2}] - [F(k) / 2 + \{F(f) + F(h)\} / \sqrt{2}] \quad (4.22)$$

The program that is used to implement edge detection runs as follows: The image from the last chapter is input to the edge detection program. The program either takes the image with a header or the image specifications can be given at run time. If no image file is specified, an image present on the screen is assumed and only its size and position on

the screen are asked for. The program allows a choice of several algorithms and requests the threshold in terms of the percent area. The algorithms that can be specified at this point are the following: Best-Fit edge operator, its extension to 3 x 3 neighborhood with weights inversely proportional to the distance, Sethi's algorithm and its extension to the *new* algorithm. The program finds all edges in the image according to the selected algorithm, and if the image is to be saved, it is thresholded according to the threshold as described above. In this application, the *new* algorithm is selected and the image is saved.

## CHAPTER 5

### CONTOUR TRACING

In analog pictures, regions of different but uniform intensities are separated by borders. An object is recognized by a sudden change in intensity level along its border. So, by finding the set of points in an analog image that undergo sudden intensity transition, an object can be located easily if the approximate shape of the object is known in advance. Points of sudden intensity transition are nothing but edges in the image. Not all edge points of an image form the boundary of the object. An edge point has to satisfy some given properties to be on the boundary. Algorithms that find the boundary vary in the specification of these properties<sup>2</sup>. Several methods have been developed to trace the contours of objects in a scene and some of them consider objects in motion [Tsu80b, Tan82, Roa80, Dar82, Hoh82]. There has also been a particular application for cardiac images in real-time [Tsu80a, Yac80]. An automated high-speed contouring system has been developed for two dimensional echocardiograms [Wei80]. In practice, however, an operator traces the approximate border of the endo- and epi-cardium in the first frame and hence it can be

---

<sup>2</sup>In digital images, the gray level values of the pixels correspond to the intensity values and the term *contour* refers to the borders.

considered only semi-automatic and operator dependent. Artificial Intelligence techniques have been applied to the study of cardiac images for recognition of the heart wall by its shape descriptors and for understanding its motion [Tso80]. Here, a few methods found in the literature for contour tracing will be described. Some of them are general methods for any object and some others were applied for the specific problem of ventricular contours in cardiac images. Towards the end of this chapter a new method is developed that combines the best features of two existing algorithms and gives surprisingly good results.

### 5.1 TRACING WITH A-MODE AND M-MODE IMAGES

This technique considers a limited search region of the display to trace the borders of epi- and endo-cardiums with A-Mode and M-Mode displays [Kuw80]. In A-Mode echocardiograms, the epicardium of the posterior wall of the left ventricle has a predominant echo and is easily identifiable. The M-Mode display gives more information on relative structures. Hence, A-Mode echoes at an instant in a cardiac cycle are recorded on a continuous M-Mode display and the position of the posterior epicardium of the left ventricle is located at that instant in the M-Mode display. The structure could move only a limited distance in a short time. So, if the contour is traced to  $C_i$ , the point  $C_{i+1}$  could only lie in a region limited by  $C_i - W_m$  and  $C_i + W_n$ .

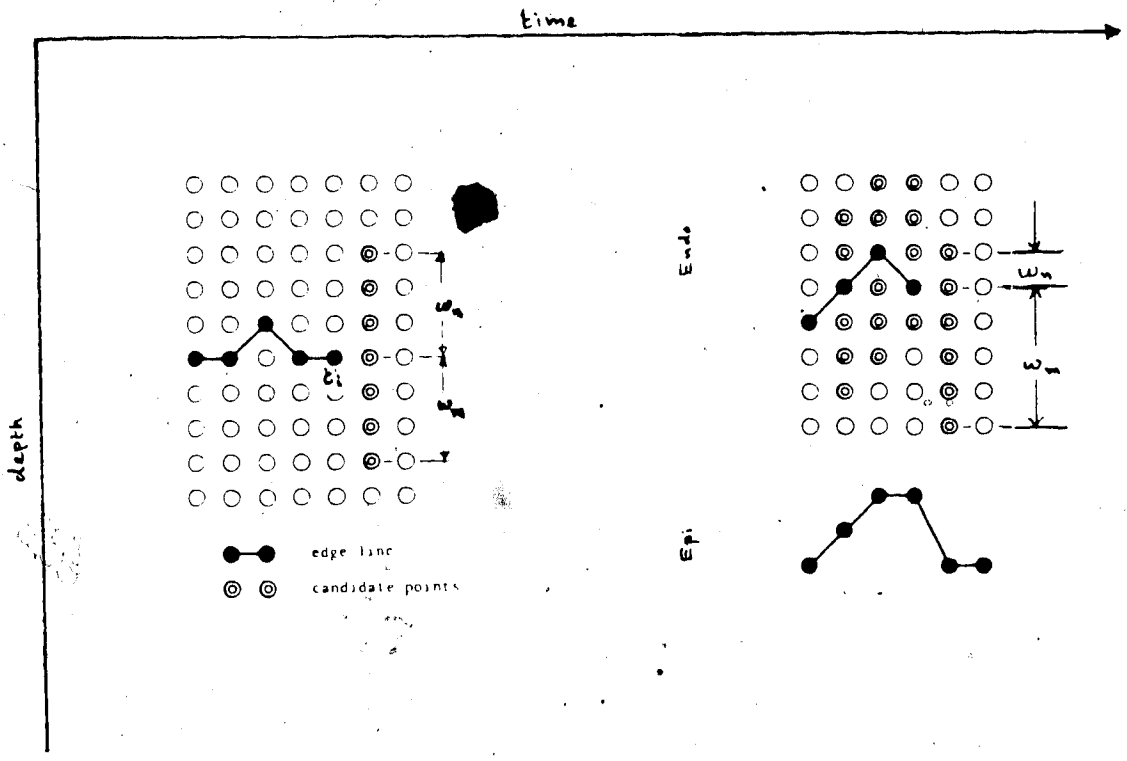


Figure 5.1 Contour tracing with A-mode and M-mode images

$W_m$  and  $W_n$  depend on the velocity of the movement of the heart wall. They are generally determined by the parameters of the EKG signal. Thus the epicardium could be traced easily. The endocardium lies within a narrow band at a distance from the epicardium but is not distinctly seen. Hence, with the help of the epicardium, the endocardium is traced within a region. The width of this region is proportional to the velocity of the wall and the region is expanded in the direction of movement. The left ventricle side of the septum is distinguishable as the epicardium is and so it is easily traced. The right ventricle side of the septum is traced following the other side of the septum as the endocardium was traced with the epicardium. The method needs only a limited region of the image to be scanned in tracing the contour of heart wall.

This method requires both M-Mode and A-Mode images to work with. The procedure should be able to correlate these two images and transform the points from A-Mode to M-Mode at appropriate places. As discussed in Chapter 2, the *motion* information obtained in this method is about the motion of the transducer and not heart wall. Hence, wall motion study cannot be really possible with this method. Also, this needs equipment for recording both M-Mode and A-Mode echoes. Contour tracing in two dimensional echocardiographic images will be more beneficial for wall motion study when done at desired EKG phases. Hence it is only appropriate to concentrate on contour tracing in two dimensional

echocardiograms.

## 5.2 CONTOURS IN THE TRANSFORMED IMAGES

There have been several approaches to the problem of contour tracing. In Nuclear Medicine [Gor81], the image is first smoothed and thresholded in a series of preprocessing steps. Then, the image is transformed from a cartesian co-ordinate system to a polar co-ordinate system to facilitate sampling along radii and to make some statistical measurements for further study. Vollmann and Mahnke approached the contour tracing problem in this manner [Vol83]. In their method, cost measures are assigned for every pixel of the image after initially smoothing and then finding the gradients. The cost value is inversely proportional to the steepness of the gradient and directly proportional to the deviation of the gray level of the pixel under consideration from the average gray level of the image. This image of cost values is then transformed to the polar co-ordinate system and the contour search problem is transformed to a minimum cost path finding problem. The minimum cost path is found by the dynamic programming method. The contour is finally retransformed to cartesian co-ordinates for display.

A technique similar to this has already been tried during this work but with no success. The results of this scheme are not reproduced here. In this technique, the

figure of merit of the pixels which is equivalent to the ~~best~~ values in the previous method is nothing but the gradient values at these points. The algorithm chooses the contour points from a narrow band with high gradient values. The initial point is selected as a point with highest gradient value in a region of specified width at a distance from the center. The failure of this method is due partly to the radial scanning of the image which had to be simulated by reading pixels along the radii of different slopes. This results in an inaccurate transformation from rectangular to polar system. Also, the transformations between two co-ordinate systems involve very high overheads. This method does not allow for contours with large breaks and with marked deviation from circular ones. Possibly, this method can collect all contour pieces and a cubic spline approximation can be done to get the full contour.

### 5.3 CONTOURS WITHOUT IMAGE TRANSFORMS

#### 5.3.1 Region Boundaries

There are a few methods that attempt to find the contour in a digital image without transforming the image. For closed contours, Pavlidis gives an algorithm that is claimed to be fast [Pav82]. A gradient image becomes a binary image after thresholding. Then the boundary can be located between the two uniform gray level regions by this



contour tracing technique. The epicardium is first traced as the object and then the endocardium is traced in a similar way as a hole in the object by reversing the color values. But, in this method, the search is guided entirely by local information and once an error is made it is propagated. There is no built-in error recovery in this technique and hence the results may not be reliable. Also, small islands are treated as holes in the object and hence this technique may end up finding any of these islands as the endocardium boundary.

### 5.3.2 Adaptive Threshold Boundary Detection

Alternatively, the boundary could be located [Liu77] in the gradient image before thresholding by picking the boundary elements i.e., points, that have

1. high contrast,
2. good connectivity, and
3. agree with some global a priori knowledge.

These three criteria form the specifications for a point to be on the boundary. The first property of high contrast is achieved by choosing points with some minimum gradient value. All points immediately around the current point are candidate points for subsequent selection to maintain continuity. The gradient value threshold is dynamically varied by finding the average of the gradient values of points that have been included in the contour set and then

taking a fixed proportion of this average. This selection method also assures the second criterion of good connectivity of boundary elements is met. When a state is reached at which the algorithm cannot find a connected point of sufficient contrast before reaching termination, the algorithm backs up far enough and then proceeds in an alternate direction. Error propagation is checked in this way before choosing the boundary elements. The algorithm is always aimed at termination which is dictated by global a priori knowledge - in this case, it is to get a closed boundary with an accepted tolerance in breakage in the contour or to start and finish with the topmost/bottommost row or the leftmost/rightmost column.

This algorithm was implemented and it was found that it does not produce acceptable results. The main drawback is that the method considers all neighbors of the current contour element without any discrimination. The algorithm is prone to serious errors because of this. When the initial point chosen lies on the contour segment of some thickness, the next point selected by the algorithm can be along the width of this segment. This selection will propagate and the algorithm may end up by tracing a small segment of the contour as the contour of the object. Secondly, because of the underlying noise in the gradient image and all neighbors of the current point are considered as candidates for the next point on the contour, the contour generated will not be smooth. In any natural object, the contours are smooth

without any drastic changes in the direction in which the consecutive elements lie. Lastly, because all neighbors are considered, the effort spent in getting the successive points of the contour is much greater than what is really needed.

### 5.3.3 Restricted Search with Fixed Threshold

Once gradients are found in a two dimensional echo display, they are thresholded by  $T_d$  to pick only the distinct changes in picture gray level values. Then, an edge tracing algorithm could be employed to fill the broken edges. In this step, another threshold  $T_x (< T_d)$  is set to select points that would lie in an edge but marginally missed. This helps in filling the gaps between pieces of the contour by natural means. A raster scan is first performed by going from bottom to top and then from left to right to cover the edges in all directions.

A scheme given by Pöppel and Herrmann can be applied to this image, instead, to get the contour and the method is described as follows [Pö82]: The contour is traced by successively going through edge values.

1. If the contour has been traced to a certain point, neighboring points that have gradient values higher than a threshold  $T_1$  and those having a larger fraction of the maximum of points 1° to 5 ( $T_2$ ), [see Figure 5.2] are considered.

		4	2	
x	x	C	1	6
		5	3	

				6
	4	2	1	
		C	3	
	x		5	
x				

		6		
	2	1	3	
	4	C	5	
		x		
		x		

x				
	x		4	
		C	2	
	5	3	1	
				6

Figure 5.2 Order of search directions

2. The steepest gradient point among 1 to 3, if any were considered, is selected as next point on the contour.
3. Otherwise, check if points 4 or 5 were considered, and select those with the larger gradient value as the next contour point.
4. Points considered but not selected until this step are stacked as they may be branch points and analyzed later.
5. If none of the points among 1 to 5 could be chosen, check if point 6 was considered after thresholding. If yes, include points 1 & 6 in the contour, 6 becoming the current point on the contour.
6. Once a dead end is reached, the points stacked at the last branch are continued with after flagging the points of the rejected branch so that they are not considered later.

Obviously, this scheme has fixed thresholds. It is difficult to find thresholds that would be good for all images as the illumination and contrast differ from image to image. Also, within the same image the threshold may vary from place to place in which case thresholds calculated for one part of the image will seriously affect the results. Otherwise, this method produces good results as the trend of the contour guides the direction of search for successive contour points. The success of this method is understood by general reasoning and from the published results, although it was not implemented in this research. The selection of thresholds may constitute one phase of this scheme by itself.

#### 5.3.4. Restricted Search with Adaptive Threshold

The drawbacks in the last two methods of contour tracing can be overcome by combining them. The concept of adaptive thresholding in the former scheme and restricting the search directions in the latter are combined to give a new scheme. The input image is specified as in earlier programs to the contour tracing program. Then, this program displays the image on the screen and prompts the user to select the initial point with a cursor and the keypad. The initial direction for search is arbitrarily assumed to be along the right horizontal axis. The program then scans other directions looking for a pixel in the direction of the

steepest gradient. The edge value at these points determine the threshold for the next candidate points. Limiting the search directions as specified by Pöppel, the next point is reached as the one with the highest gradient greater than 40% of the current threshold. The proportion, 40% of the new average, gives the threshold for finding the next point on the contour as described in Liu's algorithm.

At any instant of the search, if all search directions are exhausted without success, the program backs up by a point in the direction it came from and tries in an alternate direction after flagging this direction as useless for later attempts. Backtracking continues until a suitable direction is found for the next move. During backtracking, the threshold is also adjusted to reflect the pixel removed from the current contour. Search specifications provide for continuing the contour even if there is a break in the contour, as long as the break is not more than one pixel. This process is repeated, with backtracking wherever necessary, until the new point is within a 5 pixel distance of the initial point. At this stage, the contour is declared successfully traced. It should be noted that the contour should have been traced to some minimum length before the termination criterion is considered.

Thus, the algorithm provides for restricted search directions, variable thresholding, backtracking and jumping of minor breaks. The results of the algorithm are given in Plates 5.1 and 5.2 when used for the images on Plates 4.4.

and 4.5 respectively and the results are very good. Contour tracing fails when there is a large gap after a point because of broken edges found during edge detection. This is a problem with the image and not with the algorithm.

#### 5.4 CONTOUR EXPANSION

Most of the preceding operations have been done on the compressed image which is not suitable for display and visual inspection. Hence, the contour should be expanded to its original size and maybe even larger. With this also in mind, the output of the contour tracing algorithm is chain encoded. With a chain code it is relatively easy to expand a line drawing with reasonable accuracy - to any power of 2. Essentially, this involves doubling of the encoded data from the previous step. The output of the contour tracing program is input to this program to produce the contour expanded to twice its size in both horizontal and vertical directions. This expansion amounts to regaining the contour of the image at the original size (256 x 256). Now, the expanded contour is superimposed on the original input image for display. Plate 5.3 shows the original image given with its contour superimposed on it. Plates 5.4, 5.5 and 5.6 present regions of interest in other frames along with their contours superimposed on them. Notice, in plate 5.6, the contour is traced only for the lower half of the ventricle which is a major drawback and is explained later.

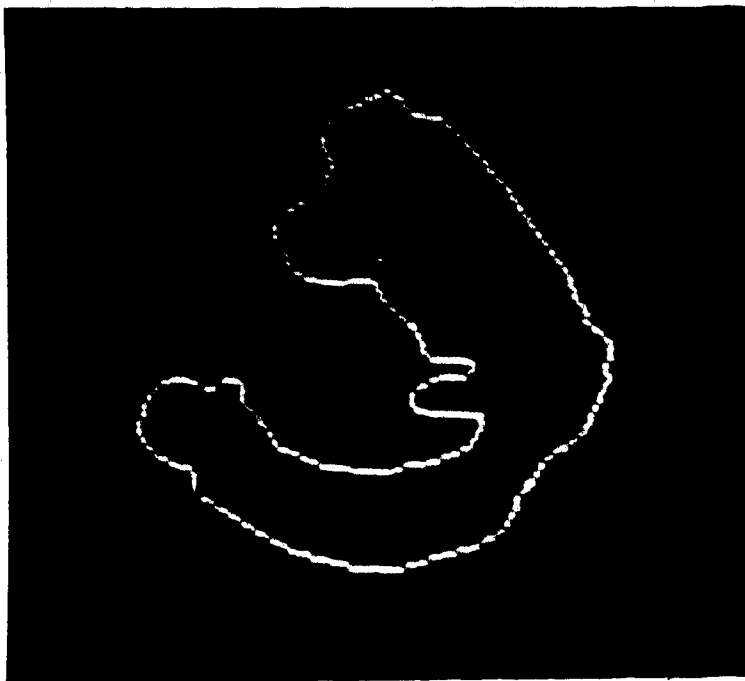


Plate 5.1 Contour for frame 1 with new algorithm



Plate 5.2 Contour for frame 2 with new algorithm



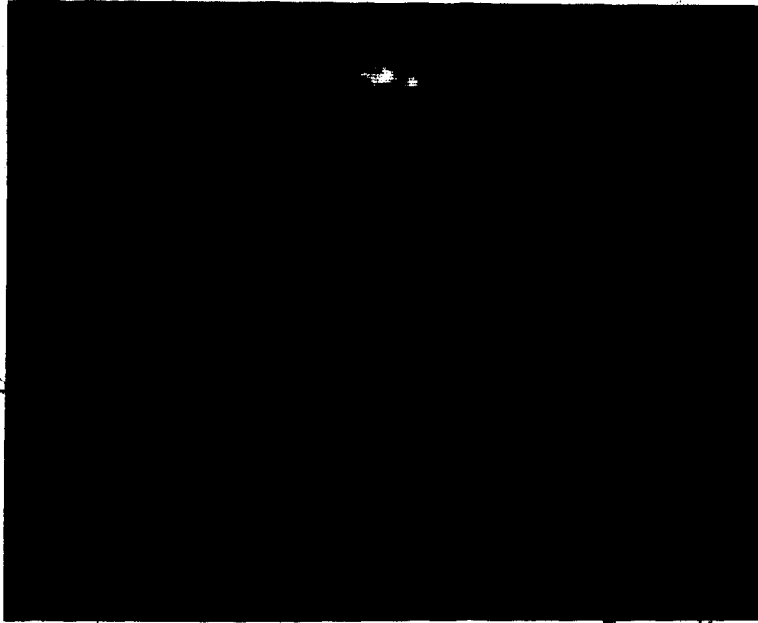


Plate 5.3 Contour superimposed on original - Frame 1



Plate 5.4 Contour superimposed on ROI - Frame 2

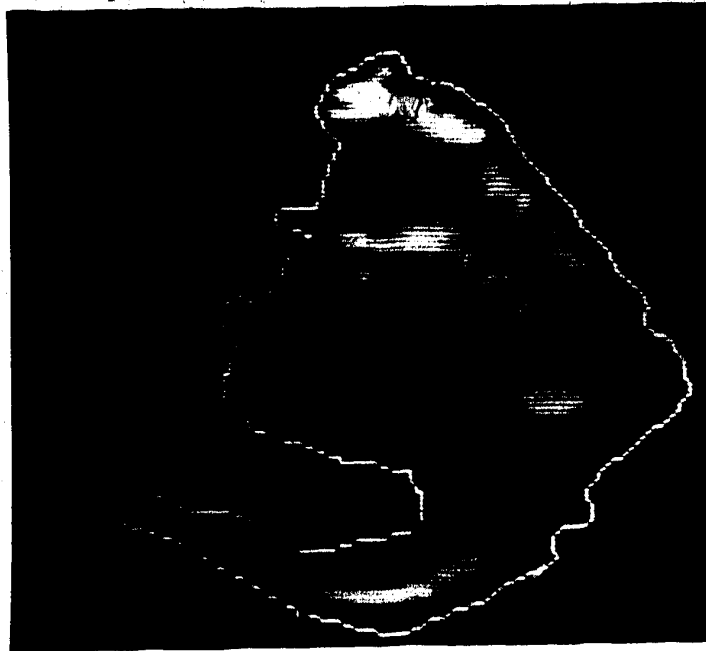


Plate 5.5 Contour superimposed on ROI - Frame 3

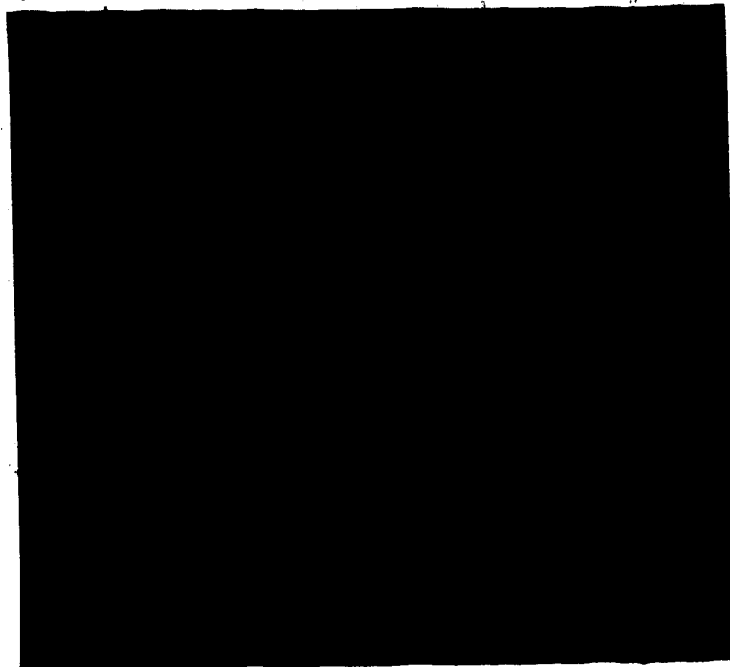


Plate 5.6 Contour superimposed on ROI - Frame 4

## 5.5 CONCLUSION

Several contour tracing schemes have been discussed. One of them operates with A-Mode and M-Mode images. Another operates on co-ordinate transformed echocardiograms and others on images without going through any transformations. Although these are general purpose contouring algorithms they can be easily adapted for two dimensional echocardiograms. Two schemes have been seen that do not involve any transforms but with drawbacks; the drawback in one being mutually resolved in another. This gives rise to a new scheme that incorporates the advantages of both of them as described in the last section. Plate 5.1 and 5.2 provide examples of the results when the new algorithm is used. A contour expansion program was described that takes advantage of the encoding scheme adopted while generating the contour. The results, when superimposed on the originals, visually show the capability of the procedure developed so far in providing outputs from poor quality input images.

## CHAPTER 6

### CONCLUSION

The research work described in this thesis will be briefly summarized. The development of various phases of the proposed procedure will be pictured in a concise manner. It will be also shown how the newly proposed method serves as a useful processing tool for echocardiograms. Limitations of the new procedure will be discussed with suggestions for overcoming them. Proposals for further research related to but beyond the scope of this research work will be presented later in the chapter.

#### 6.1: STUDY OF THE CURRENT STATE OF ART

In any image processing environment, enhancing the quality of image under study is usually the first consideration. The deterioration in quality is due to various factors like equipment, environment etc. Several algorithms that attempt noise filtering in digital images were studied with this concern in mind. Non-linear techniques based on local statistics of pixels, such as mean, were promising because of their inherent characteristics for retention of edges. Therefore averaging with and without weights assigned to neighboring pixels was studied considering different

neighborhoods. While most noise filters produced visually attractive results, the results of further processing did not warrant these very sophisticated filters. A filter with an unweighted average over a  $3 \times 3$  neighborhood was chosen for its simplicity, speed and satisfactory outputs to preprocess the images under consideration.

The next step in the recognition of objects in a scene is concerned with edge detection. Several edge operators that are currently in use were studied with their relative merits and demerits. Most of these edge detectors are based on slope information at each point of the image in some way. The best among the reported edge operators is one due to Sethi [Set82] that has an analogy to electrostatic charges. It gives strong edges compared to all other operators that were considered although the edges have discontinuities at some places.

After the edges of an object in a scene are found, the actual recognition of the object consists of discarding unwanted edge information and connecting the ones that are of interest. The edges of interest are those that have potential in forming the boundary of the object. A method was proposed in the literature that first scans the edge image and then converts the problem of contour finding to a problem of minimum path finding. The minimum path finding problem can be easily solved by dynamic programming techniques. Given a point on the contour, another method examines all its surrounding edges to get the next point on

the contour based on the steepness of these edges and a threshold. The threshold is dynamically modified depending on the edge values of contour points that have been found until the current one. Alternatively, the threshold is fixed and only a restricted set of directions are searched for consecutive contour points. The order of directions searched is based on the current direction of progress. Neither of these latter two methods are complete in locating the contour successfully and efficiently.

## 6.2 CONTRIBUTION OF THIS RESEARCH TO IMAGE PROCESSING

During the study of existing image processing techniques for solution in different phases of the enhancement of echocardiograms, methods were proposed that are either extensions or combinations of the existing ones.

There are noise filtering methods based on spatial separation of pixels in the neighborhood of a pixel. Generally, this neighborhood is of a predetermined size and the shape is usually a rectangle or a square. A noise filtering scheme proposed in this thesis considers a neighborhood of arbitrary shape whose intensity is homogeneous and whose average intensity deviates least from that of the pixel under consideration. A measure of the pixel values in this arbitrarily shaped neighborhood replaces this pixel. The measure could be a weighted average of the pixels in this neighborhood; the weights are based on gray level separation

of the pixels. In the proposed scheme, however, unweighted averaging is done over the chosen neighborhood. Thus, noise filtering by averaging the pixels over a neighborhood the shape of which is chosen on the basis of separation of gray level values is a novel way and it gives surprisingly good results.

The edge operators described in the literature basically differ from one another in the manner in which the gradients are calculated. Each operator has a way of assigning weights to the neighbors before computing the differences. Some operators are symmetric about the point at which the gradient is computed and they are generally preferred for this property. The Gradient at a point can be considered equivalent to the electrostatic potential at this point if the pixels around this are considered equivalent to electric charges. Hence, the electrostatic potential computed at a point would be a nearest approximation to the gradient at that point. i.e., the weights assigned to the neighbors should be inversely proportional to the square of their distances from the center. This method has been reported by Sethi [Set82]; but, it only resolves the gradients in the horizontal and vertical directions at a point of the image. Gradients that have high values along directions diagonal to the axes would be missed in this scheme upon thresholding. This results in broken edges especially in diagonal directions and makes contour tracing very difficult. So, it is only appropriate if the edges

aligned along other two directions are also detected before thresholding. The newly proposed method does exactly this by computing the gradients in all possible eight directions with respect to every point. This operator was implemented and found to produce good results in the class of images considered.

Contour tracing algorithms deal with only picking up edges that lie on the border of the object. They differ in the criteria adopted to select the edge points from the gradient images. Points with maximum gradient values generally picked first and this condition is gradually relaxed depending on the success in obtaining the next point on the contour. But, in any case, the value of the gradient has to be above a threshold and the specification of the threshold varies from one method to other. Liu's method [Liu77] has the capability to dynamically change this threshold and the value of the threshold is based on the gradient values of the contour points that have been accumulated so far. It suffers, however, from the drawback of looking into every point surrounding the current point. Alternatively, Pöppel's method [Pöp82] specifies the order of directions to search for the next contour point depending on the direction of progress of the contour. But, this method fails in adequately specifying the threshold value. It rather assumes a fixed threshold for the candidate points to satisfy in order to become a contour point. Both of these methods have, however, a nice property of sufficiently



backtracking when the contour reaches a dead end. The proposed algorithm takes advantage of this common backtracking property. It is combined with the dynamic threshold specification found in Liu's method and the specification of the order of search directions as given by Pöppel. Thus, it is a combination of existing algorithms using their best properties, but with their drawbacks removed. The new algorithm was used in ventricular border finding and has produced excellent outputs with the test images.

### 6.3 CRITICAL REVIEW

Upon close examination of the proposed algorithms certain flaws could be revealed. Throughout this work only square neighborhoods were considered. Square filters are not isotropic and so the measurements done later in the process should be corrected. Instead, circular neighborhoods could have been considered for smoothing or the two dimensions of the image could have been treated differently. The interested reader may refer to the method described in [Gon77]. Only those algorithms or implementation of any existing algorithm where there is an error will be discussed here. However, in future studies these deficiencies should be given very careful consideration.

The gray level weighted filter considers only the neighbors that differ least from the center for averaging. Suppose there is a line in the image with a discontinuity measuring one pixel and the discontinuity coinciding with the center of the neighborhood. The algorithm will omit the pixels forming the parts of the line and consider only the rest of the pixels for averaging if their gray level values are very close to that of the center. If the gray levels of these pixels are less than the center, the new value assigned to the center will be less than its original value. Essentially, this assignment increases the break in the edge. So, this algorithm has a tendency to produce broken edges in the image on further processing.

Histogram stretching before the edge detection step cannot be fully justified from functional point of view. If the pixel value at a point  $(x,y)$  is  $F(x,y)$ , the response of a linear edge operator at that point would be proportional to

$$\sum_N K_{xy} F(x,y) \quad (6.1)$$

where  $K_{xy}$  are the weights assigned to the neighbors by the edge operator and  $N$  is the neighborhood which the pixels belong to. After histogram stretching as described in section 4.2, the pixel value  $F_1(x,y)$  at a point  $(x,y)$  can be given as

$$F_1(x,y) = C F(x,y) + A \quad (6.2)$$

where  $C$  and  $A$  are constants.

Because the edge operation is done on the histogram stretched image, the final edge image can be expressed as

$$F_2(x,y) = C \sum_N K_{xy} F(x,y) + A \sum_N K_{xy} \quad (6.3)$$

It is apparent from equations (6.1) and (6.3) that the difference in the output of edge detection on images before and after histogram stretching is an increase in brightness of the overall image. Thus, it can be seen that though histogram stretching improves the appearance of the image very much, it only decreases the threshold value chosen during edge detection for retaining continuity. By properly changing the threshold, contour tracing would have given similar results even without this step, viz., histogram stretching. Thus, histogram stretching may be considered a functionally redundant step.

The newly proposed edge operator was shown to be biased towards the diagonal edges as those edges are amplified in comparison to the axial edges. This bias is a possible reason for diagonal slicing of the edges observed in test images. Slicing of edges may later lead to failure by contour tracing algorithms.

#### 6.4 LIMITATIONS OF THE PROPOSED PROCEDURE

It would be better if the human interaction in an image processing procedure is kept to a minimum to hasten processing. It can be seen that there are two places in the proposed procedure where human interaction is involved. First, the identification of the region of interest is done by the operator using either a graphic tablet or a keypad. Second, the initial point on the contour is chosen

interactively by the operator for tracing the heart walls. They do not, however, make the analysis subjective as the input at these places influence the analysis very little.

When there are large gaps in the image of the heart wall, contour tracing cannot successfully trace the contours. This problem is aggravated when there are more than one such break in the contour. Referring to Plate 5.3, though the tracing started at a point on the outer side of the wall, after a while, the outer side is merged with the inner one. So, tracing continues with the inner side until a certain point where it reaches the other end of the break and both sides of the wall again merge together. At this point the program switches to the outer side of wall and the contour is declared complete when the termination criterion is met. On careful observation, it is clear that it is not due to the failure of the algorithm but rather due to the frame considered for processing.

Plate 5.6 is another example where the contour traced is entirely different from what is needed. As can be seen in Plate 5.6, the image merges with the background at both right and left hand sides in the middle of the image. If contour tracing is initiated at the bottom of this frame, the program would trace the contour only for the bottom half as shown; the right side of the wall being connected to the left side by valve leaflets. Producing such wrong contours is a major drawback in this procedure. The result would be similar when the initial point is selected somewhere in the

top half of the image. The algorithm has detected a closed object though it may not be a relevant one. The drawback, however, is not due to the failure of the algorithm but rather due to the quality of the chosen frame.

#### 6.5 DIRECTIONS FOR FURTHER RESEARCH

The operator interactions mentioned above could be avoided by slightly changing the procedure. It is observed that the center of the ROI roughly coincides with the center of the screen and hence, selection of the center of ROI can be done automatically. Pixel values are checked over a narrow width at the boundary of the 256 x 256 matrix with its center at the center of screen. If the pixel values near the border coincide with those at the center, i.e. the background, then it can be assumed the object is chosen correctly. Otherwise, some part of the heart wall is on the boundary and some minor adjustments should be made for containing the whole object within the boundary. This will involve trial and error in some acute examples but should generally work well for most of the image frames.

The second human interaction takes place in the procedure for the selection of a starting point in contour tracing. As mentioned in the introduction, a study of echocardiograms considers a large number of images. These images are corrected for translational and rotational movements. They are then aligned for the study of wall

dynamics. The methods to accomplish these corrections and alignment are beyond the scope of this research project and therefore will not be discussed. Once alignment is done, the gradient images can be positioned such that the center of the left ventricle coincides approximately with a predefined point on the screen. Then, the program could scan a strip of predefined width in a prespecified direction and take the point at which the gradient is maximum as a starting point. When the program fails along one direction, it could try in several other alternate directions. But, the width of the strip as well as its location from the center of the ventricle depends on the phase of the EKG to which the frame belongs. When a series of frames are given for analysis, the procedure should start with a frame at a certain phase of the EKG. The number of frames per EKG cycle can be fixed beforehand. The heart wall is thicker near the end-systole than near the end-diastole. The wall is nearer the center at end-systole than at end-diastole. With this idea about the thickness of the wall and its anticipated location, the width of the strip can be made to vary gradually, starting with a value determined by the phase of EKG the initial frame belongs to. With this idea the location of the strip can also be adjusted from frame to frame.

There have been anomalies noted during the discussion of the results regarding the merger of the outer and inner sides of heart walls as well as the wall not being traced in a single continuous piece. This is mainly due to the fact

that the frames chosen are arbitrary in nature and the images themselves have such breaks. If several frames of the echocardiogram are taken at the same phase, but from different cycles of the EKG, the gap in one frame can be filled with the information from the neighboring frames. The frames need not be exactly at the same phase and some error is tolerated. While recording the echocardiograms, the EKG can be used to gate the data being recorded and only a fixed number of frames per cardiac cycle is allowed for recording. In case of lack of such a facility, the EKG recorded on the echocardiograms could be used for selecting synchronized frames for processing. Hence, it is to be noted that the acquisition of data plays a crucial role in the processing of echocardiograms and sufficient attention should be paid during the data collection phase of echocardiogram processing.

## REFERENCES

- .... "Ultrasound Basics, Instrumentation and Recording Techniques", in *Practical Echocardiography*.
- Bro76. Brower, R.W. and Meester, G.T., "Computer based methods for quantifying Regional Left Ventricular Wall Motion from cine-ventriculograms", *Computers in Cardiology*, vol. 55, IEEE, 1976.
- Bur82. Burt, P.J., Yen, C., and Xu, X., "Local Correlation measures for Motion Analysis, a Comparative Study", *Proceedings of the Pattern Recognition and Image Processing*, IEEE Computer Society, June, 1982 p. 269.
- Cha73. Chaitman, B.R., Braxton, J.D., and Rahimtoola, S.H., "Left Ventricular Wall Motion Assessed by Using Fixed External Reference System", *Circulation*, vol. 48, p. 1043, 1973.
- Coo82. Cook, L., Goin, J., Rosenthal, S., and Dwyer, S., "A Survey of Volume Algorithms used in Medical Applications", *Proceedings of the Pattern Recognition and Image Processing Conference*, IEEE Computer Society, 1982.
- Dar82. Darmon, C.A., "A New Recursive Method to Detect Moving Objects in a Sequence of Images", *Proceedings of the Pattern Recognition and Image Processing Conference*, IEEE Computer Society, June, 1982 pp 259-261..
- Dav79. Davis, W.A. and Orthner, R.J., "Digital Filtering for Boundary Smoothing in Digital Thematic Maps", *Proceedings of the 6th Man-Computer Communications Conference*, May, 1979.
- Deh81. Dehmer, G.J. and Firth, B.G. et al., "Direct Measurement of Cardiac output by Gated Equilibrium Blood Pool Scintigraphy: Validation of Scintigraphic Volume Measurements by a Non-Geometric Technique", *American Journal of Cardiology*, vol. 47, p. 1061, 1981.
- Deh82. Dehmer, G.J. and Firth, B.G. et al., "Non-Geometric Determination of Right Ventricular Volumes from Equilibrium Blood Pool Scans", *American Journal of Cardiology*, vol. 49, Jan 1982.
- Ell79. Elliott, H., Cooper, D.B., and Symosek, P., "Implementation, Interpretation and Analysis of a Sub-optimal Boundary Finding Algorithm", *Proceedings of the Pattern Recognition and Image Processing Conference*, pp. 122-129, IEEE Computer Society, 1979.



- Fol79.Folland, E.D. et al., "Assessment of Left Ventricular Ejection Fraction and Volume by Real-time Two Dimensional Echocardiography", *Circulation*, vol. 60, p. 760, 1979.
- Gel79.Gelberg, H.J., Brundage, B.H., Glantz, S., and Parmley, W.W., "Quantitative Left Ventricular Wall Motion Analysis: A Comparison of Area-Chord and Radial Methods", *Circulation*, vol. 59, p. 991, 1979.
- Gon77.Gonzalez, R.C. and Wintz, P., *Digital Image Processing*, Addison Wesley, 1977.
- Gor81.Goris, M.L., Sue, J., and Johnson, M.A., "A principled approach to the circumferential method for Thallium Myocardial Perfusion Scintigraphy Quantitation", *11th Annual Symposium on the Shaping of Computer Programs and Technology in Nuclear Medicine*, The society of Nuclear Medicine, 1981.
- Gue81.Guert, P., Meergaum, S., and Gordy, E. et. al., "Differential effects of Nitropruside on Ischemic and Non-Ischemic Myocardial segments demonstrated by Computer Assisted Two Dimensional Echocardiography", *American Journal of Cardiology*, vol. 48, July, 1981.
- Hab80.Haber, K., "Diagnostic uses of Ultrasound Imaging", in *Imaging for medicine*, ed. Dennis D Patton, pp. 342-348, Plenum Press, 1980.
- Hee79.Heeschen, R. and Joseph, R. et al., "Image Processing in Computed Tomography", *Proceedings of the Pattern Recognition and Image Processing*, pp. 356-362, IEEE Computer Society, 1979.
- Hoh82.Hohue, K.H. and Bohn, M., "The Processing and Analysis of Radiographic Image Sequences", *Proceedings of the Pattern Recognition and Image Processing Conference*, IEEE Computer Society, October 1982.
- Hwa82.Hwang, J.J., Lee, C.C., and Hall, E.L., "Segmentation of Solid Objects using Global and Local Edge Coincidence", *Proceedings of the Pattern Recognition and Image Processing Conference*, IEEE Computer Society, 1982.
- Ing80.Ingles, N.B., Daughters, G.T., Stinson, E.B., and Alberman, E.L., "Evaluation of Methods for Quantitative Left Ventricular Segmental Wall Motion in Man using Myocardial Markers", *Circulation*, vol. 61, 1980.
- Ing78.Ingles, N.B., Daughters, G.T., Stinson, E.B., and Alberman, E.L., "A New Method for Assessment of Left Ventricular Segmental Wall Motion", *Computers in*

*Cardiology*, vol. 57, IEEE, 1978.

- Kru80.Krush, K.R. et al., "Comparison of 19 Quantitative Models for Assessment of Localized Left Ventricular Wall Motion Abnormalities", *Clinical Cardiology*, vol. 3, 1980.
- Kuw80.Kuwahara, M. and Eiho, S. et al., "Computer Analysis of Ultrasonic Echocardiograms", in *Real-time Medical Image processing*, ed. Rosenfeld, pp. 41-52, Plenum Press, 1980.
- Led79.Ledley, R.S. and Park, C.M. et al., "Automatic Radiographic Feature Enhancement", *Proceedings of the Pattern Recognition and Image Processing Conference*, pp. 363-375, IEEE Computer Society, 1979.
- Lee80.Lee, J.S., "Digital Image Enhancement and Noise Filtering by Use of Local Statistics", *IEEE Transactions on Pattern Recognition and Machine Intelligence*, pp. 165-168, March 1980.
- Liu77.Liu, H.K., "Two and Three Dimensional Boundary Detection", *Computer Graphics and Image Processing*, vol. 6, pp. 123-134, 1977.
- Mil82.Miller, J.G. and Sobel, B.E., "Cardiac Ultrasonic Tissue Characterization", *Hospital Practice*, Jan 1982.
- Nag79.Nagao, M. and Matsuyama, T., "Edge Preserving Smoothing", *Computer Graphics and Image Processing*, vol. 9, pp. 394-407, 1979.
- Nev80.Nevatia, R. and Babu, K.R., "Linear Feature Extraction and Description", *Computer Graphics and Image Processing*, vol. 13, no. 3, 1980.
- Ove79.Overton, K.J. and Weymouth, T.E., "A noise reducing preprocessing Algorithm", *Proceedings of the Pattern Recognition and Image Processing Conference*, pp. 498-507, IEEE Computer Society, 1979.
- Pav82.Pavlidis, T., *Algorithms for Graphics and Image Processing*, Computer Science Press, 1982.
- Pel82.Peli, T. and Malah, D., "A study of Edge Detection Algorithms", *Computer Graphics and Image Processing*, vol. 20, no. 1, Sep 1982.
- Pom71.Pombo, J.F., Troy, B.L., and Russel Jr., R.O., "Left Ventricular Volume and Ejection Fraction by Echocardiography", *Circulation*, vol. 43, p. 480, 1971.
- Pop82.Poppel, S.J. and Herrman, G., "Boundary Detection in

- "Scintigraphic Images", *Computer Graphics and Image Processing*, vol. 19, no. 4, pp. 281-290, Aug 1982.
- Ram76.von Ramm, O.T. and Thrustone, F.L., "Cardiac Imaging using a Phased Array Ultrasonic System", *Circulation*, vol. 53, p. 262, 1976.
- Roa80.Roach, J.W. and Aggrawal, J.K., "Determining the Movement of Objects from a Sequence of Images", *IEEE Transactions on Pattern Analysis and Machine Intelligence*, pp. 554-562, Nov 1980.
- Roe73.Roellinger Jr, F.X., Kahveci, A.E., and Chang, J.K. et. al., "Computer Analysis of Chest Radiographs", Technical Report IAC-TR-20-73, Image Analysis Laboratory, University of Missouri, Columbia, July 1973.
- Ros76.Rosenfeld, A. and Kak, A., *Digital Image Processing*, Academic Press, 1976.
- Set82.Sethi, I.K., "Edge Detection using Charge Analogy", *Computer Graphics and Image Processing*, vol. 20, no. 2, pp. 185-195, 1982.
- Sko81.Skorton, D.J., McNary, C.A., and Child, J. et al., "Digital Image Processing of Two Dimensional Echocardiograms: Identification of the Endocardium", *The American Journal of Cardiology*, vol. 48, p. 479, Sep 1981.
- Tan82.Tang, I.S., Snyder, W.E., and Rajala, S.A., "Extraction of Moving Objects in Textured Dynamic Scenes", *Proceedings of the Pattern Recognition and Image Processing Conference*, IEEE Computer Society, 1982.
- Tom77.Tomita, F. and Tsuji, S., "Extraction of multiple regions by smoothing in selected neighborhoods", *IEEE Transactions on Systems, Man and Cybernetics*, vol. SMC 7, 1977.
- Tso80.Tsotsos, J.K., Mylopoulos, J., Covvey, H.D., and Zucker, S.W., "A Framework for Visual Motion Understanding", *IEEE Transactions on Pattern Analysis and Machine Intelligence*, pp. 563-572, Nov 1980.
- Tsu80.Tsuji, S. and Yachida, M., "Efficient Analysis of Dynamic Images Using PLANS", in *Real-time Medical Image Processing*, ed. Rosenfeld, Plenum Press, 1980.
- Tsu80.Tsuji, S., Osada, M., and Yachida, M., "Tracking and Segmentation of Moving Objects in Dynamic Line Images", *IEEE Transactions on Pattern Analysis and Machine Intelligence*, pp. 516-521, Nov 1980.

- Ven77.Venkatramanan, S.R., "Computer Analysis of Finger Prints", Master's Project, Indian Institute of Science, Bangalore, India, 1977.
- Vol3..Vollmann, W. and Mahnke, G., "Automatische Kontourfindung in Ultraschallbildern des Herzens", *5th DAGM Symposium, Karlsruhe*, Oktober, 1983..
- Wei80.Weiss, J.L., Jenkins, R.E., and Garrison, J.B., "An Automated High Speed Contouring System for Two Dimensional Echocardiography", *Clinical Research*, vol. 28, p. 220A, 1980.
- Won79.Wong, R.Y. and Hall, E.L., "Edge Extraction of Radar and Optical Images", *Proceedings of the Pattern Recognition and Image Processing Conference*, pp. 150-153, IEEE Computer Society, 1979.
- Won81.Wong, M., Shah, P.M., and Taylor, R.D., "Reproducibility of Left Ventricular Internal Dimensions with M Mode Echocardiography: Effects of Heart Size, Body Position and Transducer Angulation", *The American Journal of Cardiology*, vol. 47, p. 1068, May 1981.
- Yac80.Yachida, M., Ikeda, M., and Tsuji, S., "A Plan-Guided Analysis of Cineangiograms for Measurement of Dynamic Behavior of Heart Walls", *IEEE Transactions on Pattern Analysis and Machine Intelligence*, pp. 537-542, Nov 1980.
- HPJ83.Hewlett-Packard Journals in general and in particular "Display system for Ultrasound Images", p.20 (Dec 1983).
- Aok84.Aoki, Private communication to the author, The University of Alberta, Edmonton, Alberta, Canada, 1984

## APPENDIX A

Efficiency is one of the important factors to be taken into account in implementing computer algorithms. Certainly, this was not forgotten in this project. A brief description will be given on the efficiency of the techniques presented in this thesis.

Most of the operations are done on basically three rows of the image moving a column at a time. This technique is used to advantage for finding the new pixel gray level at a point by smoothing algorithms. First three rows are read in, and after the new values are computed at all points in the center row, new values are read into row 1. The rows are then renamed to avoid copying the values from one row to another. It may seem simple to subtract the gray values of the pixels at the leftmost column and then add those of the pixels at the next column in finding the average of a neighborhood resulting in just 6 additions. Here, all the pixels of a row are kept in an array and for every new neighborhood the values are read from the arrays for computing the average. Though this results in 3 more additions, it was retained to make the program easy and simple to understand.

The edge detection program was implemented to code the output in packed form, run length encoded form and pseudo run length encoded form. These are of much use in just displaying the edge image in binary form. The binary image

has either bright or dark pixels. The bright pixels are represented by a one and dark pixels by a zero. Then, eight pixels can be packed into a byte and the storage will be reduced to one eighth of what is otherwise required. To further reduce the storage, only the run lengths of ones and zeros are stored in an edge image. While a definite data reduction ratio can be achieved in packing the pixels of the edge image, no such predetermined ratio can be achieved in run length encoding. This occurs because the reduction depends very much on the details of the image.

Alternatively, pseudo run length encoding was tried. When there is a change in gray level by a run of length one, this change is neglected and the former run is continued as though there is no change. This definitely reduces the data storage, especially in an image of very short and broken edges, but at the cost of poor image reproduction. Hence, the pseudo run length encoding was not a big success.

When the edge image is input to a contour tracing algorithm, it is not a binary image. Instead, as mentioned earlier, gradients above a threshold are retained as they are and only those below the threshold are darkened. No encoding method is possible at this point as there is no knowledge about the threshold value. The output of the contour tracing program has to be expanded to the original size for easy recognition of the ventricle in the original image. To facilitate this, direction encoding is adopted for the output of the contour tracing program. Zero is assigned

to the positive x-direction and subsequent integers are assigned to every 45 degree increment in counterclockwise direction. Though this coding requires only 3 bits per pixel on the contour one byte was assigned because the contour is not very long; the contour data always occupies less than 2 disk blocks.